

Cytomegalovirus Induces Stage-Dependent Enamel Defects and Misexpression of Amelogenin, Enamelin and Dentin Sialophosphoprotein in Developing Mouse Molars

Tina Jaskoll^a George Abichaker^a Khine Htet^a Pablo Bringas, Jr.^b
Scott Morita^a Parish P. Sedghizadeh^c Michael Melnick^a

^aLaboratory for Developmental Genetics, ^bCenter for Craniofacial Molecular Biology, and ^cOral and Maxillofacial Pathology, Division of Periodontology, Diagnostic Sciences and Dental Hygiene, University of Southern California, Los Angeles, Calif., USA

Key Words

Cytomegalovirus-induced enamel defects · Amelogenin · Enamelin · Dentin sialophosphoprotein gene · Dentin sialoprotein

Abstract

Of the approximately 8,400 children born each year in the US with cytomegalovirus (CMV)-induced birth defects, more than one third exhibit hypoplasia and hypocalcification of

tooth enamel. Our prior studies indicated that CMV severely delayed, but did not completely interrupt, early mouse mandibular first molar morphogenesis in vitro. The aim of the present study was to examine the effects of CMV infection on progressive tooth differentiation and amelogenesis. Since initial CMV infection in human fetuses can occur at different developmental times, we varied the stage of initial viral infection (that is, Cap stage, Early Bell stage and Bell stage), as well as the duration of infection. CMV infection of embryonic mouse mandibular first molars in vitro induces

Abbreviations used in this paper

AI	amelogenesis imperfecta	Enam	enamelin gene
Amelx	amelogenin gene	FCS	fetal calf serum
CL	cervical loop	FN	fibronectin
CMV	cytomegalovirus	Fn1	fibronectin gene
CMV Bell	Bell stage-infected molars	hCMV	human cytomegalovirus
CMV Cap	Cap stage-infected molars	HERS	Hertwig's epithelial root sheath
CMV E. Bell	Early Bell stage-infected molars	mCMV	mouse cytomegalovirus
CONT	control	NBF	neutral buffered formalin
DEJ	dentino-enamel junction	PNN	probabilistic neural network
DPM	dental papilla mesenchyme	qRT-PCR	quantitative reverse transcriptase polymerase chain reaction
DSP	dentin sialoprotein	SR	stellate reticulum
DSPP	dentin sialophosphoprotein		
EGFR	epidermal growth factor receptor		

tooth dysmorphogenesis and enamel defects in a developmental stage- and duration-dependent manner. Cap stage- and Early Bell stage-infected molars exhibit enamel agenesis and Bell stage-infected molars exhibit enamel hypoplasia. This viral-induced pathology is coincident with stage-dependent changes in *Amelx*, *Enam* and *Dspp* gene expression, distribution of amelogenin, enamelin and DSP proteins, cell proliferation localization and dedifferentiation of secretory ameloblasts. Importantly, our data indicate that specific levels of *Amelx* and *Dspp* gene expression define whether mouse CMV induces enamel agenesis or hypoplasia.

Copyright © 2010 S. Karger AG, Basel

Introduction

Congenital cytomegalovirus (CMV) infection is a major cause of birth defects [for reviews, see Pass, 2005, 2007; Schleiss, 2006; Schleiss and Choo, 2006; Tsutsui, 2009; www.cdc.gov/cmvi]. It is estimated that approximately 2% of live born infants are congenitally infected with active CMV, with about 10% of this group having newborn symptoms [Syridou et al., 2005]. Approximately 80% of symptomatic newborns exhibit sequelae, including mental retardation, hearing loss and blindness, and 8–15% of infants who are asymptomatic at birth will later develop complications. Congenital CMV infection also causes tooth defects; approximately 36% of infants with CMV-induced birth defects and 5% of CMV-infected asymptomatic infants will exhibit enamel hypoplasia and hypocalcification [Stagno et al., 1982, 1983, 1984; Stehel and Sanchez, 2005]. Thus, about 1 in 1,400 live births in the US will exhibit CMV-induced amelogenesis imperfecta (AI), nearly 6 times more common than all genetic AI combined (approx. 1/8,000) [for review, see Witkop, 1988]. In many cases, the enamel is absent and affected teeth tend to wear down rapidly or to fracture. Although these distinct defects of amelogenesis are mostly reported in primary teeth, enamel defects may also be expected in the permanent dentition, since active CMV infection persists in many infants for 6–18 months postnatal. Thus, it can be estimated that approximately 3,000 children with CMV-induced AI are born each year in the US, with a prevalence to age 12 of more than 30,000. This is a significant oral health problem in that children have incisal and cuspal attrition, as well as rampant dental caries, and may require orthodontic therapy due to caries-induced loss of primary teeth [Stagno et al., 1982, 1983].

Tooth development is a continuous process during which the oral epithelium, a derivative of surface ecto-

derm, thickens and buds into the underlying neural crest-derived ectomesenchyme, and then grows and folds to form several crown shapes of varying complexity. During development, instructive and reciprocal epithelial-mesenchymal interactions result in the differentiation of ectomesenchymal cells into odontoblasts and epithelial cells into ameloblasts, which deposit dentin and enamel matrixes, respectively [for reviews, see Thesleff, 2003; Tummers and Thesleff, 2009]. The dental epithelium governs tooth development prior to the bud stage [Mina and Kollar, 1987; Lumsden, 1988] and the dental papilla regulates tooth shape and ameloblast differentiation in the Cap and Bell stages [Kollar and Baird, 1969, 1970]. Epithelial-derived pre-ameloblasts induce adjacent dental neural crest-derived ectomesenchymal cells to elongate into odontoblasts and secrete the matrix that forms pre-dentin and dentin. This in turn induces the pre-ameloblasts to polarize and differentiate into ameloblasts.

Presently, little is known about the mechanism underlying human CMV (hCMV)-induced AI. The strict species specificity of hCMV and the inability of CMV to cross the placenta of mice and rats have hindered the study of this virus [for reviews, see Pass, 2005, 2007; Kern, 2006]. Since mouse CMV (mCMV) has many features in common with hCMV and has been widely employed for studying the postnatal pathogenesis associated with acute, latent and recurrent infections [Krpmotic et al., 2003], we employed the well-established embryonic mouse tooth organ culture system to study the effects of mCMV infection on early tooth morphogenesis [Jaskoll et al., 2008a]. Our prior studies demonstrated that mCMV dysregulation of key signaling pathways disrupted early stages of tooth morphogenesis and histodifferentiation in vitro [Jaskoll et al., 2008a]. However, what remained unclear was whether mCMV infection of embryonic mouse mandibular first molars in vitro results in enamel defects similar to those seen in congenitally infected children.

The aim of the present study was to examine the effects of mCMV infection on progressive tooth differentiation and amelogenesis in cultured embryonic mandibular mouse first molars. Since initial CMV infection in human fetuses can occur at different developmental times (for example, early fetal period, late fetal period, perinatal period), we varied the stage of initial viral infection (that is, Cap stage, Early Bell stage, Bell stage) as well as the duration of infection. We postulated that the later the tooth-developmental stage of initial mCMV infection, as well as the shorter the duration, the less abnormal the anatomic phenotypes, and that these differences will be correlated with notable stage-dependent differences in

transcript and protein expression. In this paper, we delineate progressive tooth development from Cap stage to Crown formation and demonstrate that mCMV infection in vitro induces tooth dysmorphogenesis and enamel defects in a developmental stage- and duration-dependent manner, and models the pathology seen in children. This viral-induced pathology is coincident with stage-dependent changes in amelogenin (*Amelx*), enamelin (*Enam*) and dentin sialophosphoprotein (*Dspp*) transcript expression, dentin sialoprotein, enamelin and amelogenin protein distribution, localization of cell proliferation, and dedifferentiation of secretory ameloblasts.

Materials and Methods

Embryonic Culture System and mCMV Infection

Female C57BL6 mice (Charles River, Wilmington, Mass., USA) were mated overnight as previously described [Melnick et al., 2006; Jaskoll et al., 2008a]; plug day = day 0 of gestation. Timed-pregnant females were sacrificed on gestation day 15 (E15) by carbon dioxide narcosis and cervical dislocation. All procedures were performed in accordance with the Institutional Animal Care and Use Committee of USC in accordance with the Panel on Euthanasia of the American Veterinary Medical Association. Embryos were dissected in cold phosphate-buffered saline, and staged according to Theiler [1989]. Mandibular first molar regions were dissected and cultured for up to 19 days using a modified Trowell method essentially as previously described [Bringas et al., 1987; Jaskoll et al., 2008a]. The medium was BGJb (Gibco Invitrogen, Carlsbad, Calif., USA) supplemented with 50 mM ascorbic acid, 50 units/ml streptomycin and penicillin and 10% fetal calf serum. Fetal calf serum was added to the medium since it has been shown to promote epithelial differentiation and amelogenesis [Young et al., 1995; Tompkins et al., 2005]. Cultures were maintained at 37°C in atmospheric conditions of 95% air and 5% CO₂. The medium was adjusted to pH 7.4 and changed daily.

For mCMV infection, we cultured E15 Cap stage mandibular first molars and incubated them for 24 h with 250,000 plaque-forming units/ml of *lacZ*-tagged mCMV RM427⁺ [Saederup et al., 1999] on culture day 0 (Cap stage), day 5 (Early Bell stage) or day 9 (Bell stage) and then in virus-free control medium for a total culture period of 15 (E15 + 15), 17 (E15 + 17) or 19 (E15 + 19) days. Controls consisted of E15 molars cultured in virus-free control medium for 12, 15, 17 or 19 days. We have previously demonstrated that after the initial 24-hour mCMV infection, the virus continues to replicate in the dental papilla mesenchyme for the entire culture period and that active mCMV infection is necessary to initiate and sustain progressive tooth pathogenesis [Jaskoll et al., 2008a]. We employed this experimental design to analyze variation in both initial stage and duration of infection in cultured E15 molars rather than in molars of different gestational ages (E15, E16 and E17) in order to reduce variation. Explants were collected and processed for whole-mount morphology, histology or immunohistochemistry as previously described [Jaskoll et al., 2008a]. For each experimental protocol, 3–10 tooth organs/treatment/day were analyzed for each assay.

Histological Analysis

Tooth organs were fixed for 4 h in Carnoy's fixative at 4°C or overnight in 10% neutral-buffered formalin (NBF) at room temperature, embedded in paraffin, serially sectioned on the mesial-distal axis of the tooth germ at 8 μm and stained with hematoxylin and eosin as previously described [Jaskoll et al., 2008a]. For semi-thin sections, control and mCMV-infected molars cultured for 19 days were fixed overnight in 10% NBF, dehydrated through graded alcohols, and embedded in JB-4 Embedding Medium (Polysciences Inc., Warrington, Pa., USA) as previously described [Davis et al., 1985]. Serial sections were cut at 6 μm with a Sorvall JB-4 microtome and stained with 0.03% toluidine blue. All sections were analyzed using a Zeiss Axioplan microscope and a digital camera.

Quantitative RT-PCR

For analysis of gene expression, quantitative RT-PCR (qRT-PCR) was conducted as previously described [Melnick et al., 2009]. Control E15 + 15 and mCMV-infected E15 molars infected on days 0 and 9 of culture were pooled (3–4 molars per independent sample). We performed qRT-PCR on 3 independent samples per treatment group. RNA was extracted and 1 μg RNA was reverse transcribed into first-strand cDNA using ReactionReady™ First Strand cDNA Synthesis Kit: C-01 for reverse transcription (Superarray Biosciences, Frederick, Md., USA). The primer sets used were prevalidated to give single amplicons and purchased from Superarray Biosciences: *Amelx* (No. PPM29897A); β -catenin (No. PPM03384A); *Cebpa* (No. PPM04674A); *Dspp* (No. PPM40292A); *Egfr* (No. PPM03714A); *Enam* (No. PPM25461A); *Fn1* (No. PPM04224A); *Nfkb1* (No. PPM02930A); *Rela* (No. PPM04224E); *Relb* (No. PPM03202A). Primers were used at concentration of 0.4 μM. The cycling parameters were: 95°C, 15 min; 40 cycles of 95°C, 15 s; 55°C, 30–40 s, and 72°C, 30 s. Specificity of the reactions was determined by subsequent melting curve analysis. RT-PCR of RNA (not reverse transcribed) were used as negative controls. GAPDH was used to control for equal cDNA inputs and the levels of PCR product were expressed as a function of GAPDH. The relative fold changes of gene expression between the gene of interest and GAPDH, or between the controls and mCMV infected, were calculated by the 2^{-ΔΔCT} method. Significant differences between mCMV-infected and control teeth were determined by Student's t test, with $\alpha = 0.01$ and the null hypothesis of R = 1. The calculated expression ratios (R) were log or arcsin transformed prior to analysis.

Probabilistic Neural Network Analysis

We used probabilistic neural network (PNN) analyses to determine the contribution of each individual gene to the discrimination between experimental groups with 100% sensitivity and specificity. As such, PNN analyses identify the relative importance (0–1, with 0 being of no relative importance and 1 being relatively most important) of specific gene expression changes that discriminate between phenotypes. It is the contextual change in expression, not the direction of change that is important in defining the molecular phenotype. The foundational algorithm we used is based upon the work of Specht and colleagues [Specht, 1988; Specht and Shapiro, 1991; Chen, 1996]. The proprietary software designed by Ward Systems Group (Frederick, Md., USA) formulates Specht's procedure around a genetic algorithm [Goldberg, 1989]. A genetic algorithm is a computational method mod-

eled on biologic evolutionary processes that can be used to find the optimum solution to a problem that may have many solutions [Holland, 1975]. These algorithms have been found to be very powerful in solving optimization problems that appear to be difficult or unsolvable by traditional methods. They use a minimum of information about the problem and they only require a quantitative estimation of the quality of a possible solution. This makes genetic algorithms easy to use and applicable to most optimization problems.

Protein Immunolocalization

NBF- or Carnoy's-fixed, paraffin-embedded mCMV-infected molars cultured for 15 days and control molars cultured for 12 or 15 days were serially sectioned at 8 μm and immunolocalization performed using polyclonal anti-amelogenin (FL-191), anti-dentin sialoprotein (M300; Santa Cruz Biotechnology, Santa Cruz, Calif., USA) and anti-enamelin (courtesy of Jan Hu, University of Michigan) antibodies and the STAT-Q Rabbit/Mouse Peroxidase-DAB staining kit (Innovex Biosciences, Pinole, Calif., USA). Controls consisted of sections incubated in phosphate-buffered saline alone. Three to five teeth per treatment group per antibody were analyzed. The data were analyzed using a Zeiss Axioplan microscope and a digital camera.

Cell Proliferation Assay

Cell proliferation in control molars cultured for 12 or 15 days and mCMV-infected molars cultured for 15 days was determined by the cell-specific localization of proliferating cell nuclear antigen (PCNA) using the Zymed mouse PCNA kit (Invitrogen Corp., Carlsbad, Calif., USA) and counterstained with hematoxylin as previously described [Jaskoll et al., 2008a]. In this experiment, the cytoplasm appears purple and PCNA-positive nuclei appear dark brown. We compared the cell-specific distribution of PCNA-positive nuclei in Cap stage-infected and Bell stage-infected molars to control E15 + 12 and/or E15 + 15 molars. For quantitation, we determined the cell proliferation indexes for 3 regions: (1) the dental papilla mesenchyme (DPM) (PCNA-positive DPM cells/total DPM cells/ mm^2); (2) stellate reticulum (SR) (PCNA-positive SR cells/total SR cells/ mm^2); (3) cervical loop (CL) (PCNA-positive CL epithelial cells/total CL epithelial cells/ mm^2). The DPM, SR and/or CL cell proliferation indexes were determined in 3 areas per section, 3 sections per tooth and 3 teeth per group. For each region, we then calculated the mean ratios per tooth and mean ratios per group. Since percent data is not normally distributed, the data was arcsin transformed before the mean ratios of mCMV-infected and controls were compared by t test. The cell proliferation indexes are presented as the fold change in mCMV-infected/controls.

Results

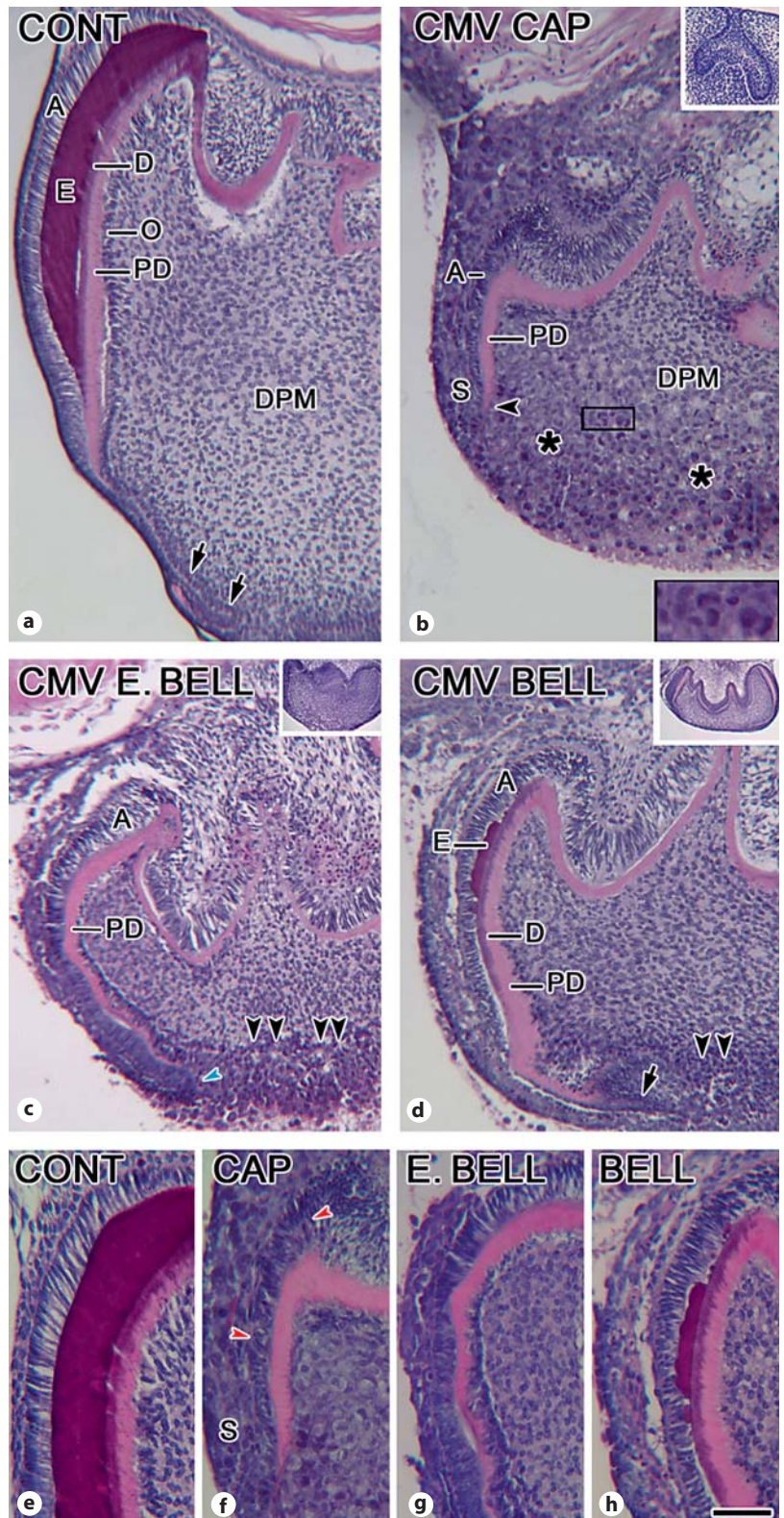
To determine if mCMV-induced enamel defects are stage dependent, we infected E15 Cap stage mandibular first molars with mCMV at the Cap stage (day 0 of culture), Early Bell stage (day 5 of culture) or Bell stage (day 9 of culture) (fig. 1b–d, insets), and cultured them for a total of 17 (fig. 1) or 19 (fig. 2) days. Exposure of embryonic

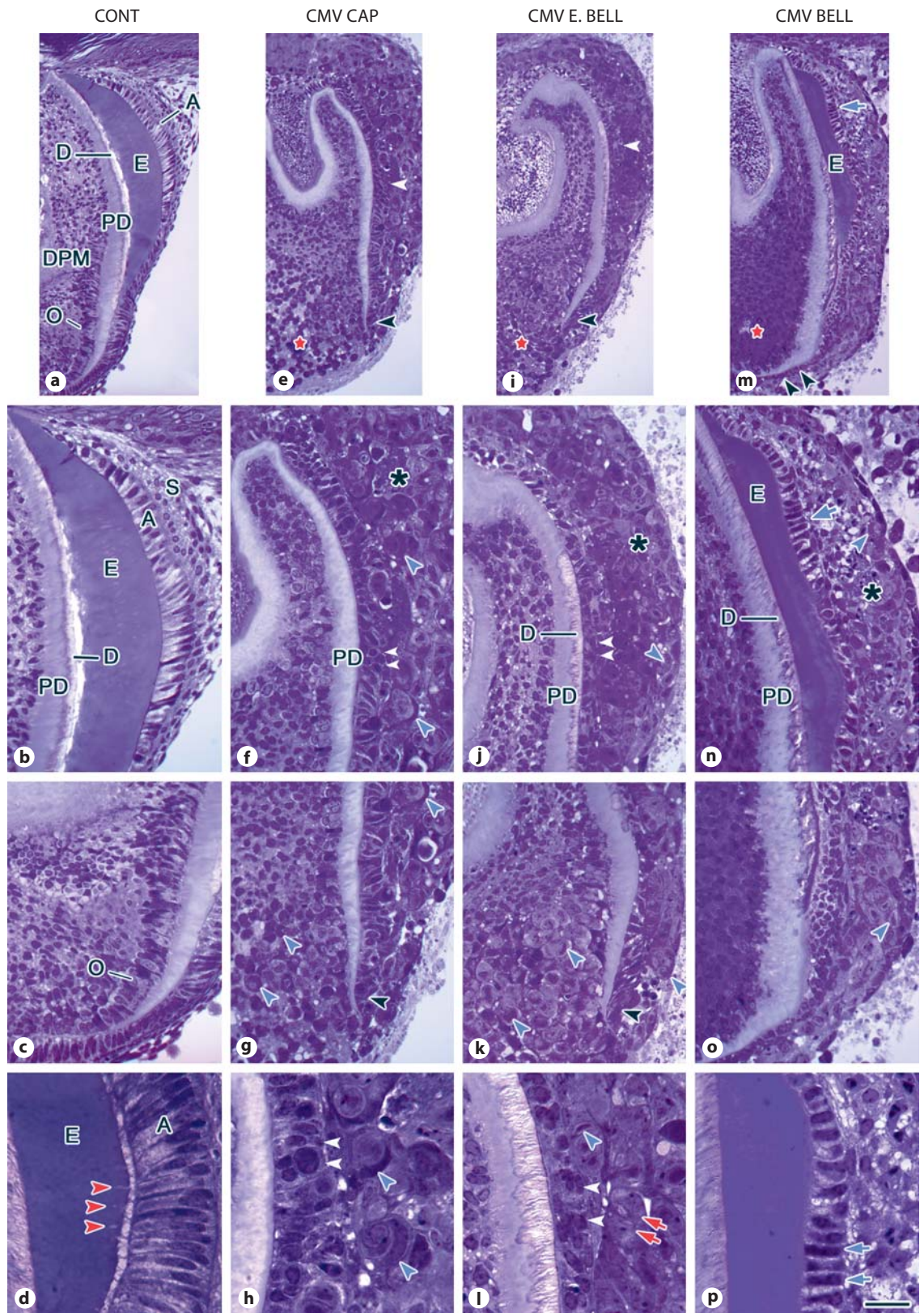
mouse molars to mCMV infection disrupted tooth morphogenesis, dentinogenesis and amelogenesis in a stage- and duration-dependent manner; the earlier the initial stage and the longer the duration of infection, the more severely abnormal the phenotype and enamel defect.

On day 17 of culture, uninfected (control) E15 Cap stage mandibular first molars have undergone normal morphogenesis and differentiation (fig. 1a, e). Dentin mineralization and formation of enamel has proceeded apically from the mesial cusp tip along the mesial side of the cusp and the dentino-enamel junction (DEJ) is readily visualized. Lobular cuspal morphology is evident coronally and root formation is seen apically, with the cervical loop extension of the inner and outer enamel epithelia bilayer forming Hertwig's epithelial root sheath (HERS).

By contrast, mCMV infection disrupts tooth morphogenesis, dentinogenesis and amelogenesis in a stage-dependent manner (compare fig. 1b–d, f–h to fig. 1a, e). Cap stage-infected molars are the most severely dysmorphic (compare fig. 1b, f to fig. 1c, d, g, h) and Bell stage-infected molars are the best developed (compare fig. 1d, h to fig. 1b, c, f, g). All mCMV-infected molars are substantially smaller compared to controls, as evidenced by the marked decrease in volume of DPM, reduced cusp tip to cervical loop length, and HERS absence or hypoplasia (compare fig. 1b–d to fig. 1a). Cap and Early Bell stage-infected molars appear more developmentally delayed and dysmorphic compared to controls than Bell stage-infected molars, as revealed by the lack of dentin mineralization and the absence of enamel matrix in these molars (compare fig. 1b, c, f, g to fig. 1a, e). Although the Bell stage-infected molars are the best developed, their phenotype is abnormal compared to controls (compare fig. 1d, h to fig. 1a, e). The infected Bell stage molars are characterized by marked decreases in mineralized dentin matrix, enamel formation, cusp size and root (HERS) formation (compare fig. 1d, h to fig. 1a, e). Although enamel matrix is seen in Bell stage-infected molars, there is limited, discontinuous enamel formation, a substantial decrease in enamel thickness, and uneven enamel matrix mineralization (compare fig. 1h to fig. 1e). In addition, the DPM in all mCMV-infected molars, regardless of stage of initial infection, appear as two distinct cell populations rather than one: round and ovoid cells within a fibromyxoid stroma, and basophilic, cytomegalic infected (some with inclusion bodies) and affected cells (fig. 1b, c, f, g). These cytomegalic infected and affected cells are more widespread in Cap stage-infected molars than in Early Bell stage molars (compare fig. 1b to fig. 1c) and in Early Bell stage than in Bell stage-infected molars (com-

Fig. 1. mCMV-induced stage-dependent differences in tooth pathology and enamel defects on day 17 of culture. **a, e** CONT: E15 mandibular first molars cultured in control medium. **b, f** CMV CAP: E15 mandibular first molars infected with mCMV at the Cap stage. **b** Upper inset: Cap stage molar. **c, g** CMV E. BELL = E15 mandibular first molars infected with mCMV at the Early Bell stage. **c** Inset: Early Bell stage molar. **d, h** CMV BELL: E15 molars infected with mCMV at the Bell stage. **d** Inset: Bell stage molar. **e-h** Representative higher magnifications of control (**e**), Cap stage-infected (**f**), Early Bell stage-infected (**g**) and Bell stage-infected (**h**) molars. **a, e** Control molars exhibit normal morphogenesis and cusp formation, characterized by polarized ameloblasts (A) and odontoblasts (O), the presence of predentin (PD), dentin (D) and enamel (E) matrixes, and the formation of HERS (**a**, double black arrows). DPM = Dental papilla mesenchyme. **b-d, f-h** mCMV infection induces smaller, developmentally delayed and dysmorphic molars compared to controls. Cap stage-infected molars (**b, f**) are the most severely dysmorphic and developmentally delayed. They are characterized by short, shallow cusps, disorganized, nonpolarized ameloblasts (**f**, red arrowheads), undifferentiated odontoblasts, a marked decrease in predentin matrix, the absence of dentin and enamel matrixes, a short, abnormal cervical loop (**b**, black arrowhead), and disorganized, multilayered stellate reticulum (S). Note the widespread distribution of basophilic, cytomegalic cells (*), some with inclusion bodies (**b**, lower inset), throughout dental papilla mesenchyme. Early Bell stage-infected molars (**c, g**) are smaller and severely dysmorphic as compared to controls but are better developed than Cap stage-infected molars. Compared to Cap stage-infected molars, they exhibit improved cusp formation, elongated ameloblasts, polarized odontoblasts, more predentin matrix, a better-developed cervical loop (**c**, blue arrowhead) and a more limited distribution of abnormal infected and affected DPM cells (**c**, double black arrowheads). Bell stage-infected molars (**d, h**) are the least dysmorphic. Compared to Cap stage-infected and Early Bell stage-infected molars, they exhibit greater cusp formation, mineralized dentin and enamel matrixes, and HERS formation. Compared to controls, Bell stage-infected molars have shorter cusps, shorter polarized ameloblasts and odontoblasts, a marked decrease in mineralized dentin matrix, and reduced HERS formation (**d**, black arrow). Although enamel is present, there is limited, discontinuous formation, reduced thickness, and uneven matrix mineralization. Note the marked decrease in abnormal affected and infected DPM cells (**d**, double black arrowheads) compared to infected Cap stage (**b**) and Early Bell stage (**c**) molars. **b-d** Scale bar = 40 μ m; **b** top inset: scale bar = 30 μ m; bottom inset: scale bar = 20 μ m; **c, d** top insets: scale bar = 160 μ m. **e-h** Scale bar = 25 μ m. The scale bar in **h** is applicable for all figures in this plate.





pare fig. 1c to fig. 1d). Note that in Cap stage-infected molars, the striking degree of infection obliterates the normal morphology and cellular architecture of the parenchyma and stroma (fig. 1b, f).

On day 19 of culture, tooth development continues to exhibit stage-dependent differences in mCMV-induced pathology (fig. 2). In control molars (fig. 2a–d), polarized odontoblasts with associated predentin and mineralized dentin are seen, and the elongated ameloblasts are polarized. Tome's processes can be seen at the secretory ends of ameloblasts inserting into the newly deposited enamel (fig. 2d), and tubules traversing through the dentin are also found (data not shown). Dental papilla cells reside in a fibromyxoid stroma and appear as round to ovoid with scant nucleoli and granular cytoplasm. The stratum intermedium is composed of 1–2 layers of cuboidal cells (fig. 2b), stellate reticulum cells reside in a myxoid stroma and appear as angulated or stellate cells with scant clear cytoplasm (fig. 2a, b), and a well-formed, elongated HERS is found (data not shown).

With mCMV infection, phenotypic changes, alterations in the integrity of epithelial and mesenchymal structures, and the presence of viral infection (viral inclusion bodies) are more profound on day 19 than on day 17 of culture (compare fig. 2e–p to fig. 1b–d, f–h). As noted above, stage-dependent differences in pathology are seen: molars infected at earlier stages are more dysmorphic than those infected at later stages (that is Cap stage

vs. Early Bell or Bell stage; Early Bell stage vs. Bell stage; compare fig. 2e–p to fig. 2a–d, fig. 2e–h to fig. 2i–p, fig. 2i–l to fig. 2m–p). Coronal morphology is disorganized and dentin mineralization is either absent (fig. 2e–h) or appears attenuated, incongruent and irregularly scalloped in many areas (fig. 2i–p); HERS is either absent (fig. 2e, g, i, k) or severely dysmorphic (fig. 2m, o). On higher magnification, it is evident that in all virally infected molars, ameloblasts, odontoblasts and DPM have lost their characteristic morphology, with odontoblasts and DPM being more severely affected (compare fig. 2f–h, j–l, n–p to fig. 2b–d). In Cap stage- and Early Bell stage-infected molars (fig. 2f–h, j–l), disorganized ameloblasts appear as blunted (often multilayered) cuboidal/low columnar cells and no enamel matrix is seen. In contrast, in Bell stage-infected molars (fig. 2n–p), ameloblasts are composed of low cuboidal or short, elongated (but not polarized) cells and appear to have a wavy structure, with enamel matrix being present. Although enamel formation is seen in infected Bell stage molars, notable enamel defects are seen compared to control (compare fig. 2m–p to fig. 2a–d). There is a marked decrease in amount of enamel matrix and length of DEJ, and Tomes' processes cannot be visualized as in controls. The enamel depth dramatically differs from control teeth, being attenuated, irregular and less abundant. In addition, the stratum intermedium and stellate reticulum are abnormal in all mCMV-infected molars, being composed of multilayers

Fig. 2. mCMV induces stage-dependent tooth defects on day 19 of culture. Semi-thin plastic sections of control and mCMV-infected molars. **a–d** Control molars (representative higher magnifications shown in **b–d**). **e–h** CMV CAP: Cap stage-infected molars (representative higher magnifications shown in **f–h**). **i–l** CMV E. BELL: Early Bell stage-infected molars (representative higher magnifications shown in **j–l**). **m–p** CMV BELL: Bell stage-infected molars (representative higher magnifications shown in **n–p**). On day 19, control molars (**a–d**) exhibit polarized odontoblasts (O) with associated predentin (PD) and mineralized dentin (D) matrixes, elongated, polarized ameloblasts (A) and associated enamel (E) matrix, and a well-developed HERS. At the secretory ends of differentiated ameloblasts, Tome's processes (**d**, red arrowheads) insert into the newly deposited enamel and tubules traverse through the dentin (data not shown). DPM cells are round to ovoid with scant nucleoli and granular cytoplasm. The stellate reticulum (S) consists of angulated or stellate cells with scant clear cytoplasm. Cap stage-infected molars (**e–h**) are the most severely abnormal. They have a multilayer of primarily cuboidal ameloblasts (white arrowhead), pleiomorphic, undifferentiated odontoblasts, predentin (but not dentin) matrix, abnormal CL/absent HERS (**e**, black arrowhead), and abnormal stellate reticulum cy-

tology. Basophilic, cytomegalic cells are seen in throughout dental papilla (**e**, red star) and stellate reticulum (**f**, *), with many of the cells exhibiting viral inclusion bodies (**f–h**, blue arrowhead). Early Bell stage-infected molars (**i–l**) are slightly better developed than Cap stage-infected molars, with taller cusps and the presence of predentin and mineralized dentin matrixes being seen. Ameloblasts are composed of a multilayer of cuboidal epithelia (white arrowhead) and HERS remains absent (black arrowhead). Basophilic, cytomegalic cells are seen in dental papilla (**i**, red star) and stellate reticulum (**l**, double red arrows), many exhibiting viral inclusion bodies (**j–k**, blue arrowhead). Bell stage-infected molars (**m–p**) are the best developed but are abnormal compared to control. Compared to controls, Bell stage-infected molars exhibit abnormal DPM (**m**, red star), shorter elongated ameloblasts (blue arrows), less mineralized dentin and predentin matrixes, enamel hypoplasia and a shorter CL/HERS (**m**, double black arrowheads). Fewer viral inclusion bodies (blue arrowhead) are seen in DPM and stellate reticulum than in Cap stage- and Early Bell stage-infected molars. **a, e, i, m** Scale bar = 50 μ m. **b, c, f, g, j, k, n, o** Scale bar = 40 μ m. **d, h, l, p** Scale bar = 27 μ m. The scale bar in **p** is applicable for all figures in this plate.

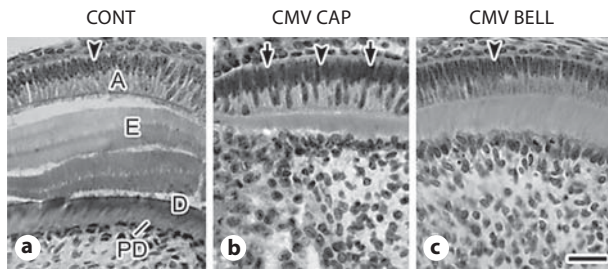
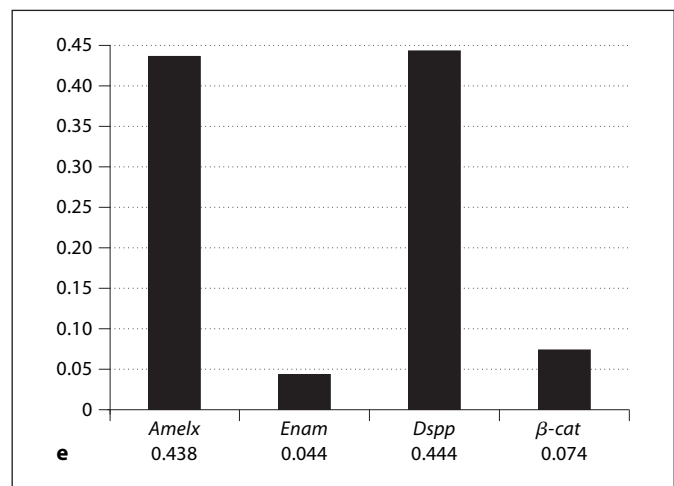
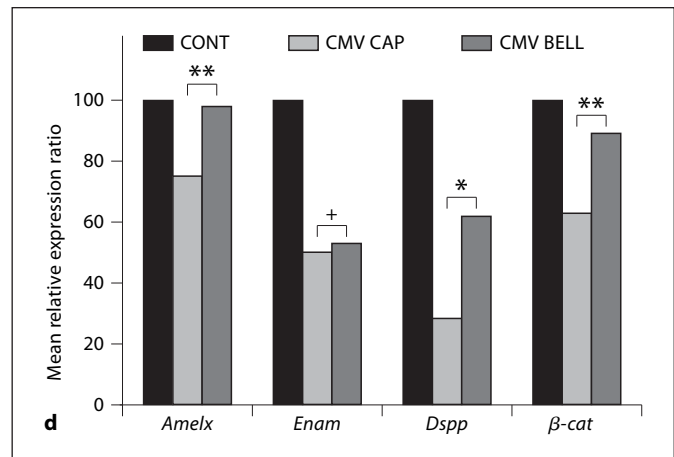


Fig. 3. Comparative *Amelx*, *Enam*, *Dspp* and β -catenin expression in control, Cap stage-infected and Bell stage-infected molars. **a–c** Ameloblast morphology in control molars (**a**), Cap stage-infected (**b**) and Bell stage-infected (**c**) molars cultured for 15 days. In control (**a**) and Bell stage-infected (**c**) molars, elongated, polarized ameloblasts (arrowhead) are found. In contrast, Cap stage-infected molars (**b**) exhibit elongated polarized (arrowhead) and nonpolarized (arrows) ameloblasts. A = Ameloblasts; D = dentin; E = enamel; PD = predentin. Scale bar = 20 μ m. **d** qRT-PCR-derived mean relative expression ratios in Cap stage- or Bell stage-infected molars compared to control molars. Differences in relative expression levels between infected Cap and Bell stage molars were calculated by t test. Brackets indicate comparisons. ** $p < 0.001$; * $p < 0.01$. + not significant. **e** PNN analysis was used to determine the contribution of each gene to the blind classification of molars as either Cap stage- or Bell stage-infected. PNN analysis identifies the relative importance (0–1, with 0 being of no relative importance and 1 being relatively most important) of specific gene expression changes that distinguish between Cap stage- and Bell stage-infected molars with 100% specificity and sensitivity. *Amelx* and *Dspp* transcript levels are relatively most important in correctly classifying molars as either Cap stage- or Bell stage-infected; *Enam* and β -cat transcript levels are relatively unimportant.



of basophilic and cytomegalic infected and affected cells (fig. 2f–h, j–l, n–p). Taken together, these findings indicate that mCMV infection results in abnormal dentinogenesis, amelogenesis and root formation, the severity of which is dependent on the developmental stage of initial infection, as well as the duration of infection.

mCMV Induces Significant Stage-Dependent Changes in Transcript Expression

Having noted the variant pathology of Cap stage- and Bell stage-infected molars after 17 and 19 days in culture (fig. 1, 2), it is critical to point out the natural history of the progressive viral-induced pathogenesis, particularly that of Cap stage-infected molars. To wit, the ameloblasts of infected Cap stage molars cultured for 15 days are elongated and mostly polarized (fig. 3b). By 17 days in culture, as noted above (fig. 1b, f), the ameloblasts are disorganized and nonpolarized, and the odontoblasts appear un-

differentiated. Thus, we chose to investigate the molecular pathology in mCMV-infected molars cultured for 15 days (E15 + 15; fig. 3b, c), that is, just prior to the histopathologic changes 48–96 h hence (compare fig. 3b, c to fig. 1f, h and fig. 2h, p). We chose infected Cap and Bell stage molars since the most abnormal tooth phenotype is evident in Cap stage-infected molars and the least abnormal phenotype in Bell stage-infected molars on days 17 and 19 of culture (fig. 1, 2).

To delineate the molecular basis for progressive mCMV-induced tooth pathology, we determined if mCMV induced stage-dependent changes in the expression of 10 molecules known to be important for tooth development, dentinogenesis and amelogenesis [Zhou and Snead, 2000; Thesleff, 2003; White et al., 2007; Hu et al., 2007, 2008; Hu and Simmer, 2007; Yamashiro et al., 2007; Gibson, 2008; Liu et al., 2008; Tummers and Thesleff, 2009] and/or shown to be involved in mCMV-

Table 1. mCMV modulation of tooth gene expression

Gene	Cap stage infected			Bell stage infected		
	R	η	p	R	η	p
<i>Dspp</i>	0.28	0.24	<0.001	0.62	0.41	<0.01
<i>Enam</i>	0.50	0.14	<0.001	0.53	0.19	<0.001
<i>Amelx</i>	0.75	0.07	<0.001	0.98	0.10	NS
<i>Cebpa</i>	1.08	0.13	NS	0.89	0.24	NS
<i>Nfkb1</i>	0.90	0.18	NS	0.67	0.22	<0.001
<i>Rela</i>	0.91	0.06	<0.01	1.13	0.13	NS
<i>Relb</i>	1.24	0.07	<0.001	0.96	0.24	NS
<i>Bcat</i>	0.63	0.18	<0.001	0.89	0.16	NS
<i>Egfr</i>	0.64	0.32	<0.001	0.62	0.18	<0.001
<i>Fnl1</i>	0.68	0.15	<0.001	0.61	0.20	<0.001

R = Mean relative expression ratio = mCMV/control (comparisons: n = 9); η = gene expression noise (0 \rightarrow 1) = S_R/R (where S_R = standard deviation of R); NS = not significantly different from control (no change in expression).

induced pathology of oral structures [Melnick et al., 2006; Jaskoll et al., 2008a, b]. We compared transcript expression in control (fig. 3a), Cap stage-infected (fig. 3b) and Bell stage-infected (fig. 3c) molars cultured for 15 days using qRT-PCR.

The results of these qRT-PCR-derived measurements are shown in table 1. For each transcript, the relative expression ratio (R) was calculated as the mean increase or decrease in gene expression in mCMV-infected teeth compared to uninfected control teeth. The variation of R is calculated as gene expression noise (η); η is statistically equivalent to the coefficient of variation and ranges from 0 to 1 [η = gene expression noise = S_R/R (where S_R = standard deviation of R)]. The value of η reflects fluctuations in promoter-binding efficiency, specific transcription factor abundance, variation in posttranscriptional modifications, and a host of other stochastic events that comprise intrinsic and extrinsic noise [Raser and O'Shea, 2005]. In the absence of prohibitively large sample sizes, as η approaches 1 it becomes extremely difficult to detect small, but potentially important, true expression differences, should they exist. Nevertheless, it is highly unlikely that substantial differences that characterize mCMV-infected tooth organs will be masked by noise. In this regard, tests of significance were determined by Student's t test, with $\alpha = 0.01$ and the null hypothesis of $R = 1$. The calculated expression ratios (R) were log or arcsin transformed prior to analysis.

mCMV induces many highly significant stage-dependent changes in the expression of genes essential for dentinogenesis and amelogenesis [*amelogenin (Amelx)*, *enamelin (Enam)*, *dentin sialophosphoprotein (Dspp)*], as well as in genes important for tooth development and altered in mCMV-infected embryonic oral structures. As shown in table 1, there are similarities, as well as differences, in transcript expression changes between infected Cap stage and Bell stage molars. Compared to controls, Cap stage-infected molars exhibit significant differences in 8 of the 10 genes, whereas Bell stage-infected molars show significant differences in 5 genes. Of genes essential for dentinogenesis and amelogenesis, both Cap stage- and Bell stage-infected molars show significant decreases in the expression of *Enam* [Cap stage: 50% ($p < 0.001$); Bell stage: 47% ($p < 0.001$)] and *Dspp* [Cap stage: 72% ($p < 0.001$); Bell stage: 38% ($p < 0.01$)]. Interestingly, only Cap stage-infected molars have a significant 25% ($p < 0.001$) decrease in *Amelx* expression, with normal levels of *Amelx* transcripts being found in Bell stage-infected molars.

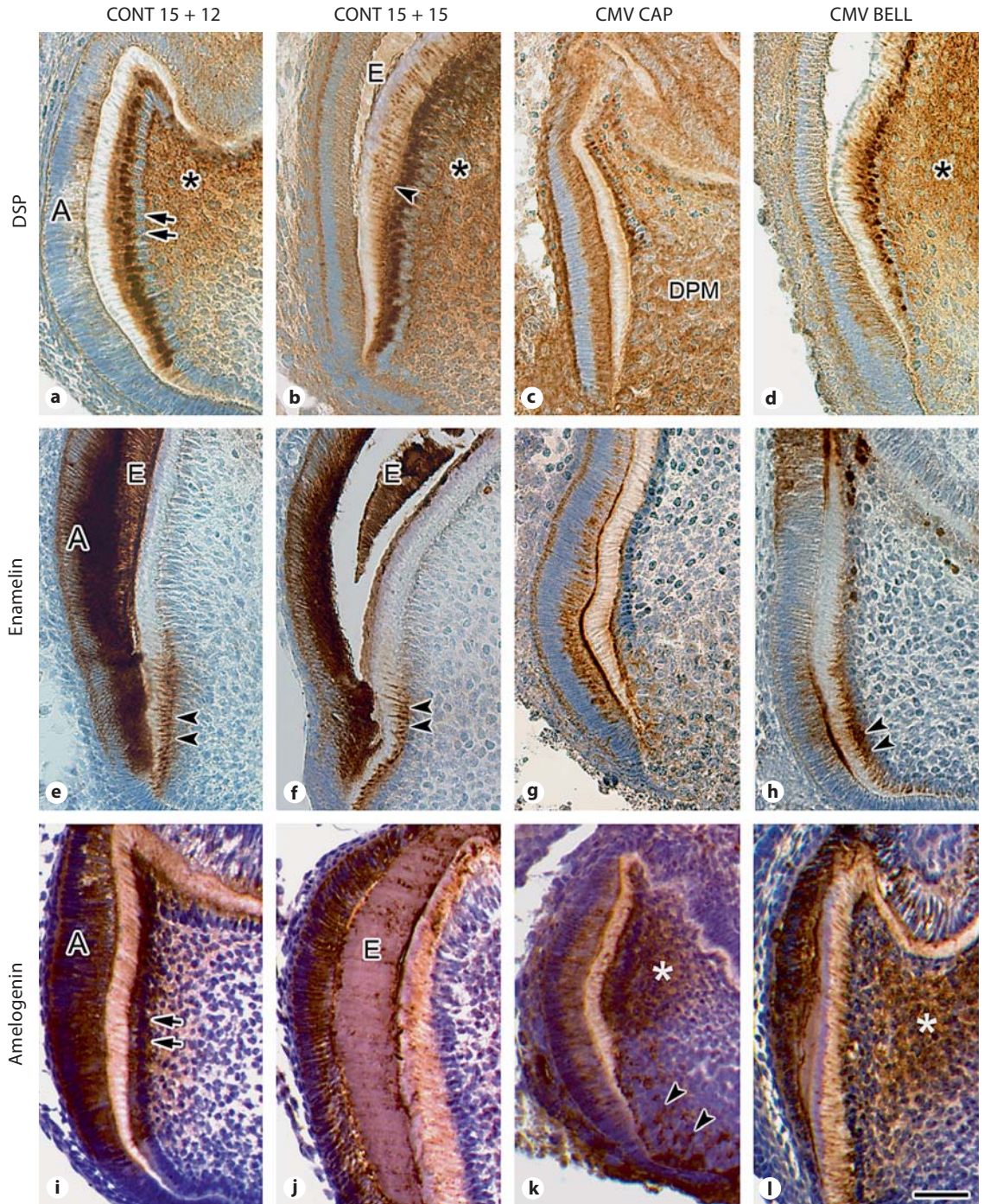
In addition, stage-dependent differences in β -catenin transcript expression are evident. Since the canonical Wnt/ β -catenin signaling is important for cusp morphogenesis, tooth shape and root formation [Yamashiro et al., 2007; Liu et al., 2008; Nemoto et al., 2009] and mCMV-infected Cap stage molars are characterized by more severely abnormal crown and root phenotypes than seen in infected Bell stage molars (fig. 1), it was reasonable to postulate that mCMV would induce greater changes in β -catenin transcript expression in Cap stage-infected molars than in Bell stage-infected molars. Our observation of a significant decrease of approximately 37% ($p < 0.001$) in β -catenin expression in Cap stage-infected molars but normal levels in Bell stage-infected molars supports this hypothesis.

Further, we also found common significant changes in the levels of specific transcripts at both stages of initial viral infection. Cap stage- and Bell stage-infected molars exhibit similar significant declines of approximately 35% ($p < 0.001$) in *Fnl1* and *Egfr* gene expression. Given that fibronectin (FN) mediates odontoblast polarization and ameloblast differentiation [Fukumoto and Yamada, 2005], EGFR is important for tooth morphogenesis and root formation [Hu et al., 1992; Fujiwara et al., 2009], and FN activation of signaling pathways is mediated via EGFR [Matsuo et al., 2006], the absence of stage-dependent changes in *Fnl1* and *Egfr* expression suggests that the FN and EGFR pathways participate during early and later stages of mCMV-induced tooth pathology.

Transcript Changes and Stage-Dependent Abnormal Phenotypes

The stage-dependent phenotypic differences in tooth morphology and enamel pathology in Cap stage- and Bell stage-infected molars are very distinct (fig. 1, 2), with enamel agenesis and hypoplasia being seen in infected

Cap stage and Bell stage molars, respectively. Given the above, we predicted sharp mathematical discrimination of the expression of genes important for enamel formation and tooth shape (*Amelx*, *Enam*, *Dspp* and β -*catenin*) among the 2 different initial stages of viral exposure. Comparisons between infected Cap stage and Bell stage



molars demonstrate that Bell stage-infected molars are 1.3-fold higher ($p < 0.001$) in *Amelx* expression, 2.2-fold higher ($p < 0.01$) in *Dspp* expression and 1.4-fold higher ($p < 0.001$) in β -catenin expression, but not significantly different in *Enam* expression, as compared to Cap stage-infected molars (fig. 3b). These results suggest that higher levels of *Amelx*, *Dspp* and β -catenin transcripts account for the better tooth morphology and enamel formation in Bell stage-infected molars as compared to Cap stage-infected molars.

We then used PNN analysis to characterize the molecular pathology with respect to the relationship of individual gene expression changes to stage of initial infection. An optimized (neural network) gene expression model was derived, resulting in a molecular signature that is able to blindly distinguish (without bias) between Cap stage- and Bell stage-infected phenotypes with 100% sensitivity and specificity. As shown in figure 3e, PNN analysis revealed that changes in *Amelx* and *Dspp* transcript expression levels are relatively most important in correctly classifying the gene expression signature as infected Cap stage molars or infected Bell stage molars. That is, our observation of enamel hypoplasia or enamel agenesis in infected Bell or Cap stage molars, respectively, is clearly defined by specific differences in *Amelx* and *Dspp* gene expression. As discussed later, this has important implications for understanding the stage-dependent differences in histopathology observed above (fig. 1, 2) and below (fig. 5).

mCMV Induces Stage-Dependent Changes in Dentin Sialoprotein, Amelogenin and Enamelin Protein Localization

Since mCMV infection clearly compromises amelogenesis and amelogenesis is dependent on sequential interactions between odontoblasts and ameloblasts, we investigated whether mCMV altered the cell-specific distribution of amelogenin and enamel proteins, the predominant proteins found in developing enamel matrix [Fincham et al., 1991], as well as dentin sialoprotein (DSP), one of the two principal dentin proteins cleaved from DSPP [MacDougall et al., 1997], in a stage-dependent manner. These three proteins have been shown to be important for enamel formation [White et al., 2007; Hu et al., 2005, 2007, 2008; Gibson, 2008; Suzuki et al., 2009]. Given our data indicate that mCMV-infected molars are developmentally delayed compared to controls, we compared the distribution of DSP, enamel and amelogenin proteins in Cap stage- and Bell stage-infected molars cultured for 15 days to control molars cultured for 12 (E15 + 12) and 15 (E15 + 15) days (fig. 4).

Analysis of DSP distribution in control E15 + 12 and E15 + 15 molars demonstrates DSP localization predominantly in the polarized, secretory odontoblasts and adjacent DPM, as well as in the polarized ameloblasts (fig. 4a, b), with increased immunostaining seen on day 15 (compare fig. 4b to fig. 4a). In E15 + 15 controls, DSP is also seen in dentinal tubules, mineralized matrix, and at the DEJ (fig. 4b). These results are similar to those previous-

Fig. 4. mCMV induces stage-dependent changes in the distribution of DSP, enamel and amelogenin proteins. **a–d** DSP localization. **e–h** Enamelin localization. **i–l** Amelogenin localization. **a–d** In E15 + 12 (**a**) and E15 + 15 (**b**) controls, DSP is strongly localized in polarized, secretory odontoblasts (double arrows) and adjacent DPM (*), and in polarized ameloblasts (**a**). In E15 + 15 controls, DSP is also found in dentinal tubules (**b**, arrowhead), mineralized matrix, and at the DEJ. E = Enamel. In Cap stage-infected molars (**c**), weak DSP immunostaining is seen in the polarized ameloblasts, stratum intermedium and stellate reticulum, as well as in abnormal odontoblasts and throughout DPM. In Bell stage-infected molars (**d**), DSP immunostaining is found primarily in odontoblasts, adjacent DPM (*), dentinal tubules and mineralized matrix, and to a lesser extent in polarized ameloblasts. **e–h**. In E15 + 12 (**e**) and E15 + 15 (**f**) controls, enamel is seen primarily in secretory ameloblasts and forming enamel; weak immunostaining is also seen in polarized odontoblasts and dentinal tubules in the DEJ region (double arrowheads). Infected Cap stage (**g**) and Bell stage (**h**) molars are characterized by markedly de-

creased enamel immunostaining in polarized ameloblasts, odontoblasts and dentinal tubules as compared to both E15 + 12 and E15 + 15 controls. **i–l** In E15 + 12 controls (**i**), strong amelogenin immunostaining is seen in secretory ameloblasts and polarized odontoblasts (double arrows), and weakly in adjacent pre-dentin and DPM. In E15 + 15 controls (**j**), strong amelogenin immunostaining is seen in polarized, secretory ameloblasts and on the DEJ; weak staining is seen in pre-dentin, dentin and enamel matrixes. In Cap stage-infected molars (**k**), mCMV induces a marked decrease in amelogenin immunostaining in ameloblasts and misexpression of amelogenin protein in odontoblasts, DPM cells in the crown area (white *), the extracellular matrix surrounding individual cytomegalic stromal cells (arrowhead), and stellate reticulum. In Bell stage-infected molars (**l**), immunostaining is localized in ameloblasts, particularly in granular-like structures in the distal parts of secretory ameloblasts, and diffusely in DPM in crown region (white *). **a–d, g–l** Scale bar = 30 μ m. **e, f** Scale bar = 40 μ m. The scale bar in **l** is applicable for all figures in this plate.

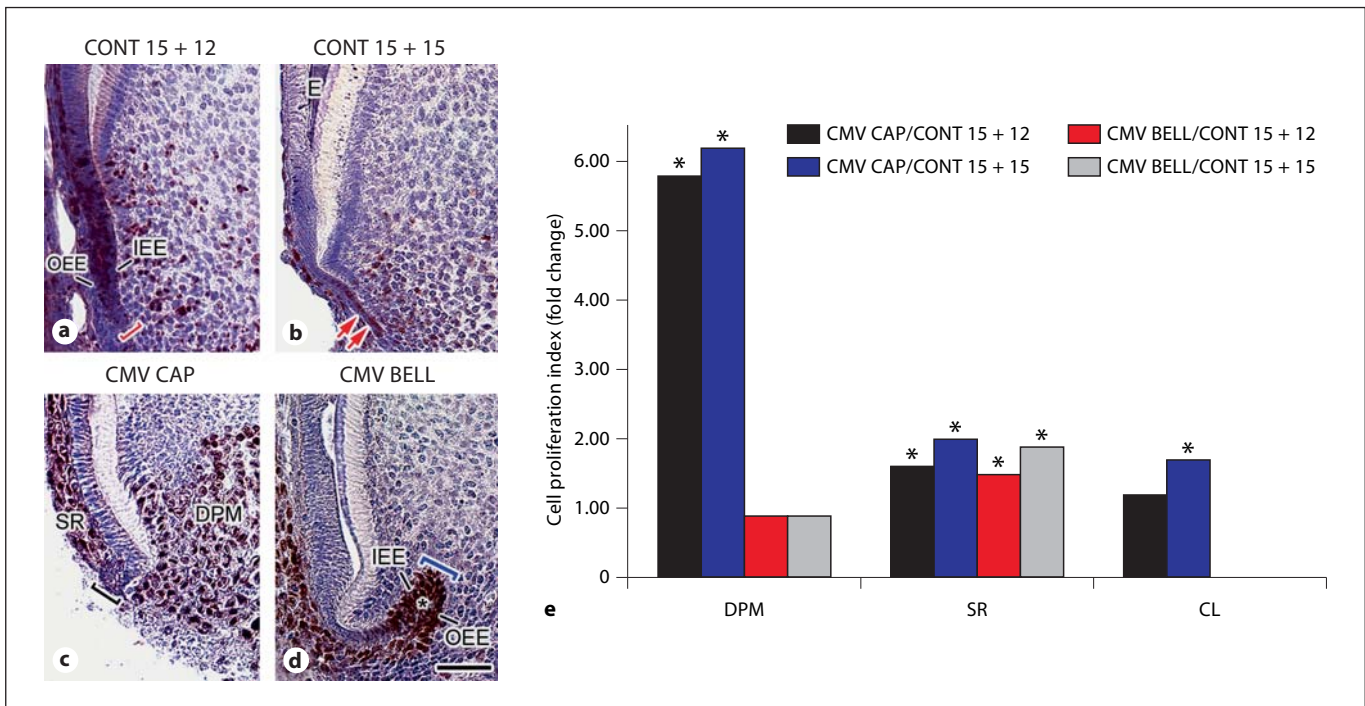


Fig. 5. mCMV-induced stage-dependent qualitative and quantitative spatial changes in PCNA localization. **a–d** The cell-specific localization of PCNA-positive nuclei in E15 + 12 control molars (**a**), E15 + 15 control molars (**b**), Cap stage-infected molars (**c**) and Bell stage-infected molars (**d**). In E15 + 12 controls (**a**), extension of the CL inner enamel epithelium (IEE) and outer enamel epithelium (OEE) forms the early HERS. PCNA-positive nuclei are seen primarily in IEE and OEE and, to a lesser extent, in surrounding mesenchymal cells and stellate reticulum. Red bracket indicates the apical end of CL/HERS. In E15 + 15 molars (**b**), PCNA-positive nuclei are seen in the fused IEE and OEE bilayer of HERS (double red arrows), in surrounding mesenchyme and stellate reticulum. E = Enamel. In Cap stage-infected molars cultured for 15 days (**c**), there is a substantial difference in the spatial localization of PCNA-positive nuclei; they are found in the cytomegalic infected and affected DPM cells but are relatively absent in the severely abnormal, hypoplastic CL (black bracket). In Bell stage-infected molars cultured for 15 days (**d**), PCNA-positive nuclei are found in the multilayered IEE and OEE of the CL (blue bracket), as well

as in the expanded population of remaining SR cells persisting between IEE and OEE (*); very few PCNA-positive nuclei are seen in DPM. In both infected Cap stage and Bell stage molars, a marked increase in PCNA-positive nuclei in the disorganized, multilayered SR cells is seen. Scale bar = 30 μ m. **e** mCMV induced stage-dependent differences in cell proliferation indexes. Cell proliferation indexes in DPM and SR of infected Cap stage or Bell stage molars were compared to E15 + 12 and E15 + 15 controls; cell proliferation indexes in CL regions of infected Cap stage and Bell stage molars were only compared to E15 + 12 controls. * Significant differences in cell proliferation indexes: (1) DPM: Cap stage-infected vs. CONT E15 + 12: 5.8-fold \uparrow ($p < 0.0001$); Cap stage-infected vs. CONT E15 + 15: 6.2-fold \uparrow ($p < 0.005$). (2) SR: Cap stage-infected vs. CONT E15 + 12: 1.6-fold \uparrow ($p < 0.0001$); Cap stage-infected vs. CONT E15 + 15: 2-fold \uparrow ($p < 0.01$); Bell stage-infected vs. CONT E15 + 12: 1.5-fold \uparrow ($p < 0.0005$); Bell stage-infected vs. CONT E15 + 15: 1.9-fold \uparrow ($p < 0.05$). (3) CL: Bell stage-infected vs. CONT E15 + 12: 1.7-fold \uparrow ($p < 0.02$) The scale bar in **d** is applicable for all figures in this plate.

ly reported [MacDougall et al., 1998; Goldberg et al., 2006; Hao et al., 2009; Yuan et al., 2009]. mCMV-infected molars exhibit a clear reduction in DSP staining intensity, as well as notable stage-dependent changes in cell-specific localization (compare fig. 4c to fig. 4a, b, d and fig. 4d to fig. 4a, b). In Cap stage-infected molars (fig. 4c), DSP is weakly localized in the polarized ameloblasts, in adjacent stratum intermedium and stellate reticulum, in polarized odontoblasts and throughout DPM. Since Bell

stage-infected molars exhibit mineralized dentin matrix and enamel formation, we expected a staining pattern somewhere between E15 + 12 and E15 + 15 controls. This is exactly what we found: DSP immunostaining is primarily found in elongated odontoblasts, dentinal tubules and mineralized matrix, and more weakly expressed in polarized ameloblasts (compare fig. 4d to fig. 4a, b). Our observation of greater differences in DSP immunostaining in Cap stage-infected molars than in Bell stage-infected

ed molars is consistent with the more severely dysmorphic DPM morphology and cellular architecture seen in Cap stage-infected molars (fig. 1, 2).

Enamelin, the largest enamel protein, is strongly localized in secretory ameloblasts (mostly in the secretory end) and forming enamel in E15 + 12 and E15 + 15 controls (fig. 4e, f); it is also weakly seen in odontoblasts and dentinal tubules in the DEJ region (fig. 4e, f). These results are consistent with previous reports [Hu et al., 2001; Nagano et al., 2003; Goldberg et al., 2005]. Importantly, mCMV induced changes in enamel localization in a stage-dependent manner (fig. 4g, h). Cap stage- and Bell stage-infected molars exhibit notable decreases in immunolocalized enamel in secretory ameloblasts and in odontoblasts, as compared to E15 + 12 and E15 + 15 controls (compare fig. 4g, h to fig. 4e, f). Enamelin is also seen in dentinal tubules in infected Bell stage (but not Cap stage) molars (compare fig. 4h to fig. 4g). Further, although the pattern of enamel immunostaining in odontoblasts and dentinal tubules in Bell stage-infected molars is similar to controls, Bell stage-infected molars show a substantial reduction in immunostaining (compare fig. 4h to fig. 4e, f).

Amelogenin, the primary protein component of enamel, is strongly localized in polarized ameloblasts and young, polarized odontoblasts, and more weakly in adjacent mesenchyme and predentin in control E15 + 12 molars (fig. 4i). In E15 + 15 control molars, strong staining is detected in polarized ameloblasts, associated with granular-like structures in the distal parts of the secretory ameloblasts and on the DEJ, weak staining is detected in enamel and dentin matrixes, and no staining is seen in mature odontoblasts (fig. 4j). These results are similar to those previously reported [Nakamura et al., 1994; Zeichner-David et al., 1997; Papagerakis et al., 2003, 2005]. mCMV induces stage-dependent changes in amelogenin protein localization (compare fig. 4k, l to fig. 4a, i, j). Compared to controls, infected Cap stage molars show reduced amelogenin immunostaining in polarized ameloblasts (compare fig. 4k to fig. 4i, j). Of particular note is the misexpression of amelogenin proteins, with amelogenins being localized in odontoblasts, DPM in the crown region and SR, as well as in the extracellular matrix surrounding apically-located cytomegalic DPM cells (fig. 4k). In infected Bell stage molars, amelogenin immunostaining is seen in elongated ameloblasts, and more weakly, in odontoblasts and adjacent DPM (fig. 4l), a distribution pattern somewhere between E15 + 12 and E15 + 15 controls (compare fig. 4l to fig. 4i, j).

mCMV Infection Induces Stage-Dependent Changes in Cell Proliferation

Since previous studies have demonstrated that mCMV infection of embryonic oral organs altered the spatial localization of proliferating cells [Melnick et al., 2006; Jaskoll et al., 2008a], we investigated whether mCMV induces stage-dependent changes in the cell-specific localization of proliferating cells in embryonic mandibular first molars in vitro. We compared the cell-specific distribution of PCNA, a marker of cells in early G1 and S phases of the cell cycle, in mCMV-infected Cap stage and Bell stage molars cultured for 15 days to control molars cultured for 12 (E15 + 12) and 15 (E15 + 15) days (fig. 5a–d). In E15 + 12 controls, PCNA-positive nuclei are primarily seen in the cervical loop extension of the inner and outer enamel epithelia which forms HERS and, to a lesser extent, in surrounding DPM and in SR cells (fig. 5a). In E15 + 15 controls, PCNA-positive nuclei are found in the well-formed HERS, in surrounding DPM and in SR cells (fig. 5b).

Since viral-induced spatial differences in cell proliferation are predicted, we compared the cell-specific distribution of PCNA-positive nuclei and the cell proliferation indexes in 3 different regions: (1) DPM (PCNA-positive DPM cells/total DPM cells/mm²); (2) SR (PCNA-positive SR cells/total SR cells/mm²); (3) CL (PCNA-positive CL epithelial cells/total CL epithelial cells/mm²). Notable stage-dependent qualitative (compare fig. 5c, d to fig. 5a, b and fig. 5d to fig. 5c) and quantitative (fig. 5e) changes are seen. Cap stage-infected molars exhibit a highly significant increase of approximately 6-fold in PCNA-positive nuclei in DPM [mCMV vs. control E15 + 12 ($p < 0.0001$); mCMV vs. control E15 + 15 ($p < 0.005$)] (compare fig. 5c to fig. 5a, b; fig. 5e); no significant differences in DPM cell proliferation are found between Bell stage-infected molars and controls (compare fig. 5d to fig. 5a, b; fig. 5e). For SR, mCMV infection induced similar significant increases of approximately 1.5–2-fold ($p < 0.05$) in cell proliferation in Cap stage- and Bell stage-infected molars (fig. 5c–e). Given that the SR of mCMV-infected Cap and Bell stage molars consists of multilayers of basophilic, cytomegalic infected and affected cells (fig. 1, 2), our data suggest that significantly increased cell proliferation on day 15 results in increased populations of abnormal SR cells seen on days 17 (fig. 1b, d) and 19 (fig. 2e–h, m–p) of culture.

In mCMV-infected molars, root development is markedly delayed and dysmorphic on day 15 of culture as compared to controls in a stage-dependent manner (compare fig. 5c, d to fig. 5a, b). Normally, after completion of crown

formation, the root (HERS) initially develops as an extension of cervical loop inner and outer enamel epithelia (fig. 5a), with depletion of the core of SR cells within the cervical loop being required for HERS formation (fig. 5b) [Thomas, 1995; Tummers and Thesleff, 2003, 2008]. However, HERS formation is not seen in mCMV-infected molars. Rather, infected Cap stage molars exhibit severely hypoplastic CL (fig. 5c); infected Bell stage molar CL are abnormal, composed of multilayered inner and outer enamel epithelia separated by an expanded population of disorganized SR cells (fig. 5d). Since a more developmentally advanced, elongated HERS is seen in E15 + 15 than in E15 + 12 controls (compare fig. 5b to fig. 5a), we compared the distribution of PCNA-positive nuclei and proliferation indexes in the CL region of mCMV-infected molars to the younger day 12 controls. With mCMV infection, notable stage-dependent differences in the CL region are seen (compare fig. 5c, d to fig. 5a, b; fig. 5e). In Cap stage-infected molars, few PCNA-positive nuclei are found in its severely hypoplastic CL (fig. 5c). This absence of cell proliferation in Cap stage-infected molar indicates that, even with additional days in culture, CL elongation to form HERS will not occur; thus, this virally induced abnormality is not merely due to developmental delay but rather to mCMV-induced histopathology. In contrast, Bell stage-infected CL exhibit PCNA-positive nuclei in the multilayered inner and outer enamel epithelia, as well as in the disorganized population of stellate reticulum cells which persist between the inner and outer epithelial layers (fig. 5d). We found a significant 1.7-fold increase ($p < 0.02$) in the CL cell proliferation index in Bell stage-infected molars as compared to controls (fig. 5e). Since cessation of cell proliferation and disappearance of SR cells in the CL is a key event regulating the timing and onset of HERS formation [Fujiwara et al., 2009], our data suggest that active cell proliferation in stellate reticulum cells in Bell stage-infected molars likely delays HERS formation.

Discussion

Tooth formation is dependent upon a coordinated series of cell-cell interactions between oral epithelium and neural crest-derived ectomesenchyme [for reviews, see Thesleff, 2003, 2006; Hu et al., 2007; Tummers and Thesleff, 2009]. Initially, odontoblasts differentiate from the ectomesenchyme and secrete predentin matrix adjacent to the epithelial-derived basal lamina. The epithelial cells then begin to elongate as differentiating ameloblasts. With the degradation of the basal lamina, the dentin ma-

trix mineralizes; sequentially, the ameloblasts deposit enamel matrix on the surface of the mineralizing dentin. Perturbation of this secretory process results in enamel agenesis or hypoplasia [for review, see Hu et al., 2007]. It is clear that in vitro mCMV infection of developing teeth compromises normal differentiation of both odontoblasts and ameloblasts, resulting in either agenesis or hypoplasia of enamel (fig. 1, 2). This in vitro mouse model provides important insight into the pathology seen in human teeth [Stagno et al., 1982]. Still, as with all in vitro models, the results presented here must be verified in vivo. Since mCMV does not cross the placenta of mice and rats, the verification continues to be a challenge [Pass, 2005, 2007; Kern, 2006].

It is well established that the phenotype of tooth pathology is dependent on the teratogen's time of initial exposure or duration of exposure [Partanen et al., 2004; Peltonen et al., 2006]. Thus, we postulated that the later the tooth developmental stage at initial mCMV infection, as well as the shorter the duration of the infection, the less abnormal the tooth phenotype will be. Our results clearly demonstrate the time (stage and duration) dependency of mCMV-induced tooth pathogenesis (fig. 1–5; table 1). Only mCMV-infected Bell stage molars, and not Cap stage- or Early Bell stage-infected molars, have enamel matrix formation, albeit hypoplastic and dysmorphic (fig. 1, 2). This mCMV-induced AI is coincident with stage-dependent differences in *Amelx*, *Enam* and *Dspp* transcript expression, localization of DSP, enamelin and amelogenin proteins, localization of cell proliferation and dedifferentiation of polarized ameloblasts, as one observes the time series from 15 (fig. 3–5) to 17 (fig. 1) to 19 (fig. 2) days in culture. Interestingly, although the ameloblast morphology seen in mCMV-infected Cap and Bell stage molars on day 15 (fig. 3) would not predict the substantial phenotypic differences seen between Cap stage- and Bell stage-infected molars on days 17 (fig. 1) and 19 (fig. 2) of culture, the major differences detected in molecular profiles (table 1; fig. 3d) foreshadows the differences seen 2–4 days later.

Dedifferentiation is the progression of cells from a more differentiated state to a less differentiated state, that is, a loss of specialization [Chen et al., 2004; Katoh et al., 2004]. After 15 days in culture, E15 tooth explants that were infected at Cap or Bell stages all exhibit ameloblasts with apically polarized nuclei and basally localized amelogenin and enamelin proteins (fig. 3, 4). Infected Cap stage ameloblasts somewhat resemble those seen in controls cultured for only 12 days, and infected Bell stage ameloblasts appear similar to controls somewhere between 12 and 15 days in culture. The presence of enamel

matrix in Bell stage-infected molars suggests that the secretory ameloblasts have been there for a longer period of time. By 19 days in culture, the Cap stage- and Early Bell stage-infected molars display ameloblasts with a cuboidal morphology characteristic of their prior undifferentiated state (fig. 2e-l); the Bell stage-infected molars display ameloblasts still elongated, but no longer polarized (fig. 2m-p). It would appear, then, that the extent of phenotype reversal is proportional to the length of time the ameloblasts were functionally differentiated. This is consistent with what has been previously well documented for dedifferentiation [Katoh et al., 2004].

Dedifferentiation is very much a regulated process involving the downregulation of developmental genes and the degradation of their extant mRNAs [Katoh et al., 2004]. Beyond this reverse of differentiation, there are gene and protein expression changes that are specific for dedifferentiation, including genes that may regulate both processes. It has been proposed that development harbors checkpoints that insure a return path to the undifferentiated state in the context of perturbation (for example mCMV infection); the checkpoint conditions developmental progression on the accumulation of a protein that is essential for dedifferentiation [Katoh et al., 2004]. Given the significant stage-dependent differences in levels of *Dspp*, *Enam* and *Amelx* transcripts in mCMV-infected molars (table 1; fig. 3) as well as marked stage-dependent changes in DSP, enamelin and amelogenin protein distribution (fig. 4), it is reasonable to speculate that DSP, enamelin and amelogenin play important roles in both differentiation and dedifferentiation of ameloblasts.

Since mCMV infection clearly compromised tooth morphogenesis and amelogenesis in a stage-dependent manner, we focused on the expression of putative ameloblast (*Enam*, *Amelx*) and odontoblast (*Dspp*) markers known to play key roles during enamel formation and mineralization [Zhou and Snead, 2000; Paine et al., 2005; White et al., 2007; Hu et al., 2007, 2008; Gibson, 2008], as well as genes important for odontogenesis and previously shown to be involved in mCMV-induced pathogenesis [Melnick et al., 2006; Yamashiro et al., 2007; Jaskoll et al., 2008a, b; Liu et al., 2008; Tummers and Thesleff, 2009]. Since common signaling pathways are utilized at different stages of tooth development [for reviews, see Thesleff, 2003; Tummers and Thesleff, 2009], we postulated that specific pathways altered at early stages would also be affected at later stages. Moreover, since the stage-dependent phenotypic differences are distinct, we also postulated sharp mathematical discrimination of gene

expression among the 2 different stages of initial viral infection.

Enamelin and amelogenin, the major protein components of enamel matrix [Fincham et al., 1991], were chosen because (1) they play essential roles in enamel formation, (2) mutations in *AMELX* and *ENAM* cause X-linked AI and autosomal dominant AI, respectively, and (3) amelogenin and enamelin null mice have abnormal teeth with disorganized, hypoplastic enamel [for reviews, see Hu et al., 2007, 2008; Gibson, 2008]. We also chose DSPP, the major noncollagenous protein in dentin matrix, since initiation of enamel matrix formation at the DEJ is associated with DSPP expression [Hu et al., 2005], mutations in *DSPP* cause various types of dental disorders [dentogenesis imperfecta (DGI) type II, DGI type III, and dentin dysplasia type II] [for reviews, see Kim and Simmer, 2007; McKnight et al., 2008] and *Dspp* null mice are characterized by abnormal teeth similar to human DGI type III [Sreenath et al., 2003]. DSPP, one of the most abundant proteins in dentin matrix, is immediately processed into two dentin matrix proteins, DSP and dentin phosphoprotein [MacDougall et al., 1997]. Both DSP and dentin phosphoprotein have been shown to play important roles during dentin and enamel formation [Paine et al., 2005; White et al., 2007; Suzuki et al., 2009; Yuan et al., 2009]. In this study, we demonstrate that mCMV infection in vitro significantly changed *Dspp*, *Enam* and *Amelx* gene expression in a stage-dependent manner (table 1; fig. 3b) and our protein localization studies (fig. 4) confirmed these results. Importantly, our observation that mCMV altered the cell-specific localization of DSP, enamelin and amelogenin proteins clearly shows the location of these molecules as they participate in normal versus abnormal enamel formation. Thus, these protein localization results provide further evidence of their pathophysiological relevance for CMV-induced AI.

Amelogenins are the most abundant secreted proteins in developing enamel matrix, comprising up to 90% of the proteins present [Fincham et al., 1991]. Since amelogenin transcripts were initially found only in ameloblasts by in situ hybridization [Nakamura et al., 1994; Karg et al., 1997; Bleicher et al., 1999; Hu et al., 2001], and enamel hypoplasia and abnormal mineralization are seen in *Amelx* null mice [Gibson et al., 2001], it was reasonably thought that amelogenins solely regulate enamel matrix formation and mineralization. However, amelogenin transcripts and proteins have also been found in odontoblasts, pulp cells and cementoblasts in developing teeth [Oida et al., 2002; Veis, 2003; Papagerakis et al., 2003, 2005], as well as in tissues not related to odontogenesis

(for example, brain cells, hematopoietic cells and chondrogenic/osteogenic cells) [for review, see Deutsch et al., 2006]. In vitro and in vivo studies have clearly demonstrated that amelogenins have signaling properties [Hoang et al., 2002; Veis, 2003; Tompkins et al., 2005, 2006; Zeichner-David et al., 2006; Ye et al., 2006; Matsuzawa et al., 2009; Warotayanont et al., 2009].

Alternative splicing of the primary mRNA transcript results in several long- and short-spliced isoforms of amelogenin [Simmer et al., 1994; Hu et al., 1997]. Iacob and Veis [2006] demonstrated that ameloblasts, odontoblasts and stratum intermedium cells each have distinct spatial and temporal patterns of amelogenin isoforms. Of particular note is the M59/[A-4] (LRAP) isoform, for which there is a putative receptor [Tompkins et al., 2005, 2006]. The [A-4] isoform is secreted by maturing mouse odontoblasts before the onset of dentin mineralization and inhibits ameloblast maturation; it is proposed that this permits a sufficiently thick layer of dentin to be produced, blocking any further epithelial-mesenchymal signaling [Tompkins et al., 2005]. When cultured E16 tooth germs are exposed to exogenous [A-4] protein, there is normal dentin matrix formation but disrupted ameloblast maturation, ranging from multiple cuboidal cells to elongated cells with indeterminate polarization [Tompkins et al., 2005]. It is proposed that the diffusion of [A-4] into the epithelial cell layer may provide a gradient opposite to that in control cultures.

Even though dedifferentiation of polarized ameloblasts as one observes the time series of Cap stage-infected molars from 15 (fig. 3, 4) to 17 (fig. 1) to 19 (fig. 2) days in culture is associated with a reduction in *Amelx* transcript expression (table 1) and misexpression of amelogenin protein in DPM (fig. 4), it remains reasonable to hypothesize that upregulation of [A-4] in the context of overall amelogenin protein decline may be driving the dedifferentiation in a manner similar to that seen in the study by Tompkins et al. [2005]. It is a recognized principle of concentration-dependent signaling that if the amount or duration of the signal is too great, development is diverted from its normal course [Freeman and Gurdon, 2002]. Even a mere 3-fold increase in ligand concentration or time of exposure will dramatically alter cell fate. Furthermore, the decrease in *Dspp* and *Enam* transcript expression, as well as in immunolocalized DSP and enamel proteins, in both infected Cap stage and Bell stage molars suggests that their downregulation also participates in dedifferentiation of ameloblasts and enamel pathogenesis.

The least abnormal tooth phenotype is seen in Bell stage-infected molars, with enamel hypoplasia (and not agenesis) being seen. This less severe pathology is associated with *Amelx* and *β-catenin* transcript expression levels similar to those seen in controls, as well as the significantly higher *Dspp* expression compared to Cap stage-infected molars. Given that canonical Wnt/ β -catenin signaling regulates tooth shape and root formation [Yamashiro et al., 2007; Liu et al., 2008; Nemoto et al., 2009], the significantly higher *β-catenin* expression in Bell stage-infected molars as compared to Cap stage-infected molars likely mediates the improved tooth morphology and root formation. Furthermore, since amelogenins activate the canonical Wnt/ β -catenin pathway [Matsuzawa et al., 2009; Warotayanont et al., 2009] and Wnt/ β -catenin signaling regulates *Dspp* transcript expression [Yamashiro et al., 2007], the significantly higher *Dspp* expression in Bell stage-infected molars may be due, in part, to the significantly approximately 25–30% higher ($p < 0.001$) *Amelx* and *β-catenin* transcript expression. Moreover, PNN analysis revealed that specific differences in *Amelx* and *Dspp* gene expression is relatively most important for distinguishing between the infected Cap stage and Bell stage enamel defect (that is, enamel agenesis vs. hypoplasia). Our results further indicate that the significant upregulation of *Amelx* gene expression to normal levels, as well as the significantly higher *Dspp* expression, in Bell stage-infected molars likely accounts for enamel formation (albeit abnormal).

Finally, our qRT-PCR-derived results also indicate that common key pathways are utilized at different stages of mCMV-induced pathogenesis. Given that FN and EGFR are important for normal tooth morphogenesis [Hu et al., 1997; Fukumoto et al., 2005], FN activation of signaling pathways is mediated through EGFR [Matsuo et al., 2006], and mCMV-induced downregulation of *Egfr* and *Fn1* expression is not stage dependent (table 1), the similar significant reductions in *Fn1* and *Egfr* expression in Cap stage- and Bell stage-infected molars suggest that the FN and EGFR pathways are involved during early and later stages of viral-induced tooth pathology. Also, given that EGFR signaling is important for the onset and timing of HERS formation [Fujiwara et al., 2009] and Wnt/ β -catenin signaling is important for root formation [Nemoto et al., 2009], the significant decrease in *Egfr* transcripts, but stage-dependent reduction in *β-catenin* expression, likely accounts for HERS agenesis or hypoplasia in infected Cap stage or Bell stage molars, respectively.

In conclusion, we have demonstrated for the first time that mCMV induces tooth pathology and enamel defects

in a stage- and duration-dependent manner: the earlier the initial stage and the longer the duration of infection, the more severely abnormal the phenotype. This viral-induced pathology is coincidental with stage-dependent changes in *Amelx*, *Enam* and *Dspp* expression, amelogenin, enamelin and DSP protein distribution, cell proliferation localization, and dedifferentiation of secretory ameloblasts. Our observation of disorganized and blunted cuboidal ameloblasts in Cap stage- and Early Bell stage-infected molars indicates that the absence of enamel formation is not merely due to developmental delay, but rather to mCMV-induced ameloblast histopathology. Finally, our data indicate that whether mCMV induces enamel agenesis or hy-

poplasia is defined by the specific levels of *Amelx* and *Dspp* gene expression. Further studies are needed to delineate the proteomic changes related to mCMV infection of mouse tooth organs. Together, these studies will reveal drug targets that will ameliorate enamel defects in the permanent dentitions of about 3,000 children born each year with CMV-induced amelogenesis imperfecta.

Acknowledgements

We would like to thank Dr. Edward Mocarski for his generous gift of mCMV and Dr. Jan Hu for her generous gift of enamelin antibodies.

References

- Bleicher, F., M.L. Couble, J.P. Farges, P. Couble, H. Magloire (1999) Sequential expression of matrix protein genes in developing rat teeth. *Matrix Biol* 18: 133–143.
- Bringas, P., M. Nakamura, E. Nakamura, J. Evans, H.C. Slavkin (1987) Ultrastructural analysis of enamel formation during in vitro development using chemically-defined medium. *Scanning Microsc* 1: 1103–1108.
- Chen, C. (ed.) (1996) *Fuzzy Logic and Neural Network Handbook*. New York, McGraw-Hill.
- Chen, S., A. Unterbrink, S. Kadapakkam, J. Dong, T.T. Gu, J. Dickson, H.H. Chuang, M. MacDougall (2004) Regulation of the cell type-specific dentin sialophosphoprotein gene expression in mouse odontoblasts by a novel transcription repressor and an activator CCAAT-binding factor. *J Biol Chem* 279: 42182–42191.
- Davis, J.U., P. Bringas, H.C. Slavkin (1985) Quantitative localization of polystyrene microspheres following microinjection in the avian metencephalic neural crest pathway. *J Craniofac Genet Dev Biol* 5: 11–19.
- Deutsch, D., A. Haze-Filderman, A. Blumenfeld, L. Dafni, Y. Leiser, B. Shay, Y. Gruenbaum-Cohen, E. Rosenfeld, E. Fermon, B. Zimmermann, S. Haegewald, J.P. Bernimoulin, A.L. Taylor (2006) Amelogenin, a major structural protein in mineralizing enamel, is also expressed in soft tissues: brain and cells of the hematopoietic system. *Eur J Oral Sci* 114: 183–189.
- Fincham, A.G., Y. Hu, E.C. Lau, H.C. Slavkin, M.L. Snead (1991) Amelogenin post-secretory processing during biomineralization in the postnatal mouse molar tooth. *Arch Oral Biol* 36: 305–317.
- Fong, C.D., L. Hammarstrom, C. Lundmark, T. Wurtz, I. Slaby (1996) Expression patterns of RNAs for amelin and amelogenin in developing rat molars and incisors. *Adv Dent Res* 10: 195–200.
- Freeman, M., J.B. Gurdon (2002) Regulatory principles of developmental signaling. *Annu Rev Cell Dev Biol* 18: 515–539.
- Fujiwara, N., T. Akimoto, K. Otsu, T. Kagiya, K. Ishizeki, H. Harada (2009) Reduction of EGF signaling decides transition from crown to root in the development of mouse molars. *J Exp Zool B Mol Dev Evol* 312B: 486–494.
- Fukumoto, S., Y. Yamada (2005) Review: extracellular matrix regulates tooth morphogenesis. *Connect Tissue Res* 46: 220–226.
- Gibson, C.W. (2008) The amelogenin 'enamel proteins' and cells in the periodontium. *Cr Rev Eukar Gene Express* 18: 345–360.
- Gibson, C.W., Z.A. Yuan, B. Hall, G. Longenecker, E. Chen, T. Thyagarajan, T. Sreenath, J.T. Wright, S. Decker, R. Piddington, G. Harrison, A.B. Kulkarni (2001) Amelogenin-deficient mice display an amelogenesis imperfecta phenotype. *J Biol Chem* 276: 31871–31875.
- Goldberg, D.E. (1989) *Genetic Algorithms in Search, Optimization, and Machine Learning*. Reading, Addison-Wesley.
- Goldberg, M., D. Septier, A. Oldberg, M.F. Young, L.G. Ameye (2006) Fibromodulin-deficient mice display impaired collagen fibrillogenesis in predentin as well as altered dentin mineralization and enamel formation. *J Histochem Cytochem* 54: 525–537.
- Goldberg, M., D. Septier, O. Rapoport, R.V. Iozzo, M.F. Young, L.G. Ameye (2005) Targeted disruption of two small leucine-rich proteoglycans, biglycan and decorin, exerts divergent effects on enamel and dentin formation. *Calcif Tissue Int* 77: 297–310.
- Hao, J., A. Ramachandran, A. George (2009) Temporal and spatial localization of the dentin matrix proteins during dentin biomineralization. *J Histochem Cytochem* 57: 227–237.
- Hoang, A.M., R.J. Klebe, B. Steffensen, O.H. Ryu, J.P. Simmer, D.L. Cochran (2002) Amelogenin is a cell adhesion protein. *J Dent Res* 81: 497–500.
- Holland, J.H. (1975) *Adaptation in Natural and Artificial Systems*. Ann Arbor, University of Michigan Press.
- Hu, C.C., O.H. Ryu, Q. Qian, C.H. Zhang, J.P. Simmer (1997) Cloning, characterization, and heterologous expression of exon-4-containing amelogenin mRNAs. *J Dent Res* 76: 641–647.
- Hu, C.C., Y. Sakakura, Y. Sasano, L. Shum, P. Bringas Jr., Z. Werb, H.C. Slavkin (1992) Endogenous epidermal growth factor regulates the timing and pattern of embryonic mouse molar tooth morphogenesis. *Int J Dev Biol* 36: 505–516.
- Hu, J.C., Y.H. Chun, T. Al Hazzazi, J.P. Simmer (2007) Enamel formation and amelogenesis imperfecta. *Cells Tissues Organs* 186: 78–85.
- Hu, J.C., Y. Hu, C.E. Smith, M.D. McKee, J.T. Wright, Y. Yamakoshi, P. Papagerakis, G.K. Hunter, J.Q. Feng, F. Yamakoshi, J.P. Simmer (2008) Enamel defects and ameloblast-specific expression in Enam knock-out/lacZ knock-in mice. *J Biol Chem* 283: 10858–10871.
- Hu, J.C., J.P. Simmer (2007) Developmental biology and genetics of dental malformations. *Orthod Craniofac Res* 10: 45–52.
- Hu, J.C., X. Sun, C. Zhang, J.P. Simmer (2001) A comparison of enamelin and amelogenin expression in developing mouse molars. *Eur J Oral Sci* 109: 125–132.
- Hu, J.C., Y. Yamakoshi, F. Yamakoshi, P.H. Krebsbach, J.P. Simmer (2005) Proteomics and genetics of dental enamel. *Cells Tissues Organs* 181: 219–231.
- Iacob, S., A. Veis (2006) Identification of temporal and spatial expression patterns of amelogenin isoforms during mouse molar development. *Eur J Oral Sci* 114: 194–200.

- Jaskoll, T., G. Abichaker, N. Jangaard, P. Bringas Jr., M. Melnick (2008a) Cytomegalovirus inhibition of embryonic mouse tooth development: A model of the human amelogenesis imperfecta phenocopy. *Arch Oral Biol* 53: 405–415.
- Jaskoll T., G. Abichaker, P.P. Sedghizadeh, P. Bringas, M. Melnick (2008b) Cytomegalovirus induces abnormal chondrogenesis and osteogenesis during embryonic mandibular development. *BMC Dev Biol* 8: 33.
- Karg, H.A., E.H. Burger, D.M. Lyaruu, J.H. Wöltgens, A.L. Bronckers (1997) Gene expression and immunolocalisation of amelogenins in developing embryonic and neonatal hamster teeth. *Cell Tissue Res* 288: 545–555.
- Katoh, M., C. Shaw, Q. Xu, N. Van Driessche, T. Morio, H. Kuwayama, S. Obara, H. Urushihara, Y. Tanaka, G. Shaulsky (2004) An orderly retreat: Dedifferentiation is a regulated process. *Proc Natl Acad Sci USA* 101: 7005–7010.
- Kern, E.R. (2006) Pivotal role of animal models in the development of new therapies for cytomegalovirus infections. *Antiviral Res* 71: 164–171.
- Kim, J.W., J.P. Simmer (2007) Hereditary dentin defects. *J Dent Res* 86: 392–399.
- Kollar, E.J., G.R. Baird (1969) The influence of the dental papilla on the development of tooth shape in embryonic mouse tooth germs. *J Embryol Exp Morphol* 21: 131–148.
- Kollar, E.J., G.R. Baird (1970) Tissue interactions in embryonic mouse tooth germs. II. The inductive role of the dental papilla. *J Embryol Exp Morphol* 24: 173–186.
- Krmpotic, A., I. Bubic, B. Polic, P. Lucin, S. Jonjic (2003) Pathogenesis of murine cytomegalovirus infection. *Microbes Infect* 5: 1263–1277.
- Liu, F., E.Y. Chu, B. Watt, Y. Zhang, N.M. Gallant, T. Andl, S.H. Yang, M.M. Lu, S. Piccolo, R. Schmidt-Ullrich, M.M. Taketo, E.E. Morrisey, R. Atit, A.A. Dlugosz, S.E. Millar (2008) Wnt/ β -catenin signaling directs multiple stages of tooth morphogenesis. *Dev Biol* 313: 210–224.
- Lumsden A.G. (1988) Spatial organization of the epithelium and the role of neural crest cells in the initiation of the mammalian tooth germ. *Development* 103 Suppl: 155–169.
- MacDougall, M., J. Nydegger, T.T. Gu, D. Simmons, X. Luan, A. Cavender, R.N. D'Souza (1998) Developmental regulation of dentin sialophosphoprotein during ameloblast differentiation: a potential enamel matrix nucleator. *Connect Tissue Res* 39: 25–37.
- MacDougall, M., D. Simmons, X. Luan, J. Nydegger, J. Feng, T.T. Gu (1997) Dentin phosphoprotein and dentin sialoprotein are cleavage products expressed from a single transcript coded by a gene on human chromosome 4. Dentin phosphoprotein DNA sequence determination. *J Biol Chem* 272: 835–842.
- Matsuo, M., H. Sakurai, Y. Ueno, O. Ohtani, I. Saiki (2006) Activation of MEK/ERK and PI3K/Akt pathways by fibronectin requires integrin α -mediated ADAM activity in hepatocellular carcinoma: a novel functional target for gefitinib. *Cancer Sci* 97: 155–162.
- Matsuzawa, M., T.J. Sheu, Y.J. Lee, M. Chen, T.F. Li, C.T. Huang, J.D. Holz, J.E. Puzas (2009) Putative signaling action of amelogenin utilizes the Wnt/ β -catenin pathway. *J Periodontal Res* 44: 289–296.
- McKnight, D.A., P. Suzanne Hart, T.C. Hart, J.K. Hartsfield, A. Wilson, J.T. Wright, L.W. Fisher (2008) A comprehensive analysis of normal variation and disease-causing mutations in the human DSPP gene. *Hum Mutat* 29: 1392–1404.
- Melnick, M., E.S. Mocarski, G. Abichaker, J. Huang, T. Jaskoll (2006) Cytomegalovirus-induced embryopathology: mouse submandibular salivary gland epithelial-mesenchymal ontogeny as a model. *BMC Dev Biol* 6: 42.
- Melnick, M., R.D. Phair, S.A. Lapidot, T. Jaskoll (2009) Salivary gland branching morphogenesis: a quantitative systems analysis of the Eda/Edar/NF κ B paradigm. *BMC Dev Biol* 9: 32.
- Mina, M., E.J. Kollar (1987) The induction of odontogenesis in non-dental mesenchyme combined with early murine mandibular arch epithelium. *Arch Oral Biol* 32: 123–127.
- Nagano, T., S. Oida, H. Ando, K. Gomi, T. Arai, M. Fukae (2003) Relative levels of mRNA encoding enamel proteins in enamel organ epithelia and odontoblasts. *J Dent Res* 82: 982–986.
- Nakamura, M., P. Bringas Jr., A. Nanci, M. Zeichner-David, B. Ashdown, H.C. Slavkin (1994) Translocation of enamel proteins from inner enamel epithelia to odontoblasts during mouse tooth development. *Anat Rec* 238: 383–396.
- Nemoto, E., Y. Koshikawa, S. Kanaya, M. Tsuchiya, M. Tamura, M.J. Somerman, H. Shimauchi (2009) Wnt signaling inhibits cementoblast differentiation and promotes proliferation. *Bone* 44: 805–812.
- Oida, S., T. Nagano, Y. Yamakoshi, H. Ando, M. Yamada, M. Fukae (2002) Amelogenin gene expression in porcine odontoblasts. *J Dent Res* 81: 103–108.
- Paine, M.L., W. Luo, H.J. Wang, P. Bringas Jr., A.Y. Ngan, V.G. Miklus, D.H. Zhu, M. MacDougall, S.N. White, M.L. Snead (2005) Dentin sialoprotein and dentin phosphoprotein overexpression during amelogenesis. *J Biol Chem* 280: 31991–31998.
- Papagerakis, P., M. MacDougall, D. Hotton, I. Bailleul-Forestier, M. Oboeuf, A. Berald (2003) Expression of amelogenin in odontoblasts. *Bone* 32: 228–240.
- Papagerakis, R., J.M. Ibarra, N. Inozentseva, P. DenBesten, M. MacDougall (2005) Mouse amelogenin exons 8 and 9: sequence analysis and protein distribution. *J Dent Res* 84: 613–617.
- Partanen, A.M., A. Kiukkonen, C. Sahlberg, S. Alaluusua, I. Thesleff, R. Pohjanvirta, P.L. Lukinmaa (2004) Developmental toxicity of dioxin to mouse embryonic teeth in vitro: arrest of tooth morphogenesis involves stimulation of apoptotic program in the dental epithelium. *Toxicol Appl Pharmacol* 194: 24–33.
- Pass, R.F. (2005) Congenital cytomegalovirus infection and hearing loss. *Herpes* 12: 50–55.
- Pass, R.F. (2007) Congenital cytomegalovirus infection: impairment and immunization. *J Infect Dis* 195: 767–769.
- Peltonen, E., P.L. Lukinmaa, C. Sahlberg, A.M. Partanen, A. Kiukkonen, S. Alaluusua (2006) 7,12-dimethylbenz[a]anthracene interferes with the development of cultured mouse mandibular molars. *Toxicol Sci* 92: 279–285.
- Raser, J.M., E.K. O'Shea (2005) Noise in gene expression: origins, consequences, and control. *Science* 309: 2010–2013.
- Saederup, N., Y.C. Lin, D.J. Dairaghi, T.J. Schall, E.S. Mocarski (1999) Cytomegalovirus-encoded beta chemokine promotes monocyte-associated viremia in the host. *Proc Natl Acad Sci USA* 96: 10881–10886.
- Schleiss, M.R. (2006) Nonprimate models of congenital cytomegalovirus (CMV) infection: gaining insight into pathogenesis and prevention of disease in newborns. *ILAR J* 47: 65–72.
- Schleiss, M.R., D.I. Choo (2006) Mechanisms of congenital cytomegalovirus-induced deafness. *Drug Discovery Today: Disease Mechanisms* 3: 105–113.
- Simmer, J.P., C.C. Hu, E.C. Lau, P. Sarte, H.C. Slavkin, A.G. Fincham (1994) Alternative splicing of the mouse amelogenin primary RNA transcript. *Calcif Tissue Int* 55: 302–310.
- Specht, D. (1988) Probabilistic neural network for classification, mapping, or associative memory. *Proc IEEE Int Conf Neural Networks* 1: 525–532.
- Specht, D., P. Shapiro (1991) Generalization accuracy of probabilistic neural networks captured with back-propagation networks. *Proc IEEE Int Joint Conf Neural Networks* 1: 887–892.
- Sreenath, T., T. Thyagarajan, B. Hall, G. Longenecker, R. D'Souza, S. Hong, J.T. Wright, M. MacDougall, J. Sauk, A.B. Kulkarni (2003) Dentin sialophosphoprotein knockout mouse teeth display widened predentin zone and develop defective dentin mineralization similar to human dentinogenesis imperfecta type III. *J Biol Chem* 278: 24874–24880.
- Stagno, S., R.F. Pass, M.E. Dworsky, C.A. Alford (1983) Congenital and perinatal cytomegalovirus infections. *Semin Perinatol* 7: 31–42.
- Stagno, S., R.F. Pass, M.E. Dworsky, W.J. Britt, C.A. Alford (1984) Congenital and perinatal cytomegalovirus infections: clinical characteristics and pathogenic factors. *Birth Defects Orig Artic Ser* 20: 65–85.

- Stagno, S., R.F. Pass, J.P. Thomas, J.M. Navia, M.E. Dworsky (1982) Defects of tooth structure in congenital cytomegalovirus infection. *Pediatrics* 69: 646–648.
- Stehel, E.K., P.J. Sanchez (2005) Cytomegalovirus infection in the fetus and neonate. *Neo Rev* 6: e38–e45.
- Suzuki, S., T. Sreenath, N. Haruyama, C. Honeycutt, A. Terse, A. Cho, T. Kohler, R. Müller, M. Goldberg, A.B. Kulkarni (2009) Dentin sialoprotein and dentin phosphoprotein have distinct roles in dentin mineralization. *Matrix Biol* 28: 221–229.
- Syridou, G., C. Skevaki, D.A. Kafetzis (2005) Intrauterine infection with parvovirus B19 and CMV: implication in early and late gestation fetal demise. *Expert Rev Anti Infect Ther* 3: 651–661.
- Theiler, K. (1989) *The House Mouse: Atlas of Embryonic Development*. New York, Springer-Verlag.
- Thesleff, I. (2003) Epithelial-mesenchymal signalling regulating tooth morphogenesis. *J Cell Sci* 116: 1647–1648.
- Thesleff, I., P. Sharpe (1997) Signalling networks regulating dental development. *Mech Dev* 67: 111–123.
- Thomas, H.F. (1995) Root formation. *Int J Dev Biol* 39: 231–237.
- Tompkins, K., K. Alvares, A. George, A. Veis (2005) Two related low molecular mass polypeptide isoforms of amelogenin have distinct activities in mouse tooth germ differentiation in vitro. *J Bone Miner Res* 20: 341–349.
- Tompkins, K., A. George, A. Veis (2006) Characterization of a mouse amelogenin [A-4]/M59 cell surface receptor. *Bone* 38: 172–180.
- Tsutsui, Y. (2009) Effects of cytomegalovirus infection on embryogenesis and brain development. *Congenit Anom (Kyoto)* 49: 47–55.
- Tummers, M., I. Thesleff (2003) Root or crown: a developmental choice orchestrated by the differential regulation of the epithelial stem cell niche in the tooth of two rodent species. *Development* 130: 1049–1057.
- Tummers, M., I. Thesleff (2008) Observations on continuously growing roots of the sloth and the K14-Eda transgenic mice indicate that epithelial stem cells can give rise to both the ameloblast and root epithelium cell lineage creating distinct tooth patterns. *Evol Dev* 10: 187–195.
- Tummers, M., I. Thesleff (2009) The importance of signal pathway modulation in all aspects of tooth development. *J Exp Zool B Mol Dev Evol* 312B: 309–319.
- Veis, A. (2003) Amelogenin gene splice products: potential signaling molecules. *Cell Mol Life Sci* 60: 38–55.
- Warotayanont, R., B. Frenkel, M.L. Snead, Y. Zhou (2009) Leucine-rich amelogenin peptide induces osteogenesis by activation of the Wnt pathway. *Biochem Biophys Res Commun* 387: 558–563.
- White, S.N., M.L. Paine, A.Y. Ngan, V.G. Miklus, W. Luo, H. Wang, M.L. Snead (2007) Ectopic expression of dentin sialoprotein during amelogenesis hardens bulk enamel. *J Biol Chem* 282: 5340–5345.
- Witkop, C.J. Jr. (1988) Amelogenesis imperfecta, dentinogenesis imperfecta and dentin dysplasia revisited: problems in classification. *J Oral Pathol* 17: 547–553.
- Yamashiro, T., L. Zheng, Y. Shitaku, M. Saito, T. Tsubakimoto, K. Takada, T. Takano-Yamamoto, I. Thesleff (2007) Wnt10a regulates dentin sialophosphoprotein mRNA expression and possibly links odontoblast differentiation and tooth morphogenesis. *Differentiation* 75: 452–462.
- Ye, L., T.Q. Le, L. Zhu, K. Butcher, R.A. Schneider, W. Li, P.K. Besten (2006) Amelogenins in human developing and mature dental pulp. *J Dent Res* 85: 814–818.
- Young, W.G., J.V. Ruch, M.R. Stevens, C. Bègue-Kirn, C.Z. Zhang, H. Lesot, M.J. Waters (1995) Comparison of the effects of growth hormone, insulin-like growth factor-I and fetal calf serum on mouse molar odontogenesis in vitro. *Arch Oral Biol* 40: 789–799.
- Yuan, G., Y. Wang, J. Gluhak-Heinrich, G. Yang, L. Chen, T. Li, L.A. Wu, Z. Chen, M. Macdougall, S. Chen (2009) Tissue-specific expression of dentin sialophosphoprotein (DSP) and its polymorphisms in mouse tissues. *Cell Biol Int* 33: 816–829.
- Zeichner-David, M., L.S. Chen, Z. Hsu, J. Reyna, J. Caton, P. Bringas (2006) Amelogenin and ameloblastin show growth-factor like activity in periodontal ligament cells. *Eur J Oral Sci* 1: 244–253.
- Zeichner-David, M., H. Vo, H. Tan, T. Diekwisch, B. Berman, F. Thiemann, M.D. Alcocer, P. Hsu, T. Wang, J. Eyna, J. Caton, H.C. Slavkin, M. MacDougall (1997) Timing of the expression of enamel gene products during mouse tooth development. *Int J Dev Biol* 41: 27–38.
- Zhou, Y.L., M.L. Snead (2000) Identification of CCAAT/enhancer-binding protein alpha as a transactivator of the mouse amelogenin gene. *J Biol Chem* 275: 12273–12280.